MCB
Journals.ASM.org

Cell Autonomous Lipin 1 Function Is Essential for Development and Maintenance of White and Brown Adipose Tissue

Karim Nadra,[a,b] Jean-Jacques Médard,[a] Joram D. Mul,[c]* Gil-Soo Han,[d] Sandra Grès,[e] Mario Pende,[b] Daniel Metzger,[f] Pierre Chambon,[f] Edwin Cuppen,[c] Jean-Sébastien Saulnier-Blache,[e] George M. Carman,[d] Béatrice Desvergne,[g] and Roman Chrast[a]

Department of Medical Genetics, University of Lausanne, Lausanne, Switzerland[a]; Inserm U845, Université Paris Descartes, Paris, France[b]; Hubrecht Institute-KNAW and University Medical Center Utrecht, Utrecht, The Netherlands[c]; Department of Food Science and Rutgers Center for Lipid Research, Rutgers University, New Brunswick, New Jersey, USA[d]; Inserm U858/I2MR, Department of Metabolism and Obesity, Team 3, Toulouse, France[e]; Institut de Génétique et de Biologie Moléculaire et Cellulaire, CNRS UMR7104, Inserm U964, Université de Strasbourg, Collège de France, Illkirch, France[f]; and Center for Integrative Genomics, University of Lausanne, Lausanne, Switzerland[g]

Through analysis of mice with spatially and temporally restricted inactivation of *Lpin1*, we characterized its cell autonomous function in both white (WAT) and brown (BAT) adipocyte development and maintenance. We observed that the lipin 1 inactivation in adipocytes of $aP2^{Cre/+}/Lp^{fEx2\text{-}3/fEx2\text{-}3}$ mice resulted in lipodystrophy and the presence of adipocytes with multilocular lipid droplets. We further showed that time-specific loss of lipin 1 in mature adipocytes in $aP2^{Cre\text{-}ERT2/+}/Lp^{fEx2\text{-}3/fEx2\text{-}3}$ mice led to their replacement by newly formed *Lpin1*-positive adipocytes, thus establishing a role for lipin 1 in mature adipocyte maintenance. Importantly, we observed that the presence of newly formed *Lpin1*-positive adipocytes in $aP2^{Cre\text{-}ERT2/+}/Lp^{fEx2\text{-}3/fEx2\text{-}3}$ mice protected these animals against WAT inflammation and hepatic steatosis induced by a high-fat diet. Loss of lipin 1 also affected BAT development and function, as revealed by histological changes, defects in the expression of peroxisome proliferator-activated receptor alpha (PPARα), PGC-1α, and UCP1, and functionally by altered cold sensitivity. Finally, our data indicate that phosphatidic acid, which accumulates in WAT of animals lacking lipin 1 function, specifically inhibits differentiation of preadipocytes. Together, these observations firmly demonstrate a cell autonomous role of lipin 1 in WAT and BAT biology and indicate its potential as a therapeutical target for the treatment of obesity.

Adipocytes and glial cells both rely heavily on appropriately controlled lipid metabolism: adipocytes in order to execute their role as "energy storage regulators" and glial cells in order to produce and maintain myelin membrane. A spontaneous null mutation in the *Lpin1* gene present in "fatty liver dystrophy" mice ($Lpin1^{fld/fld}$) affects both cell types, leading to a progressive demyelinating peripheral nerve neuropathy and marked lipoatrophy (27, 28, 39, 57).

Lipin 1 is a Mg^{2+}-dependent phosphatidic acid phosphatase (PAP1), an enzyme necessary for normal lipid biosynthesis (11, 18). An absence of PAP1 activity in $Lpin1^{fld/fld}$ mice results in dysregulated triacylglycerol biosynthesis and a subsequent accumulation of phosphatidic acid (PA) in white adipose tissue (WAT) and peripheral nerve endoneurium, which mediates part of the $Lpin1^{fld/fld}$ demyelination phenotype (36). The systemic loss of PAP1 activity and resulting impairment in triacylglycerol synthesis also clearly contribute to the lipodystrophy in $Lpin1^{fld/fld}$ mice (13). Recently, we described a rat model with a mutated *Lpin1* protein ($Lpin1^{1Hubr}$) lacking PAP1 activity that developed hypomyelination and mild lipodystrophy (34). On the contrary, overexpression of *Lpin1* in adipose tissue promotes obesity when mice are fed a high-fat diet (40). Importantly, reduced levels of *Lpin1* mRNA were observed in subjects with obesity, insulin resistance and HIV-associated lipodystrophy (29, 53, 56), while mutations in *LPIN1* were recently found to result in recurrent childhood episodes of myoglobinuria (33, 64). These *in vivo* observations, together with the data showing that lipin 1 is involved in adipogenesis *in vitro* (25, 38, 42), suggest that lipin 1 plays an important role in adipocyte development and function. But *in vivo* adipose tissue-specific inactivation of lipin 1 has not been explored so far.

In order to characterize the cell autonomous function of lipin 1 in adipocyte maturation, maintenance, and survival, we selectively deleted *Lpin1* in developing and mature adipocytes through the use of time- and tissue-specific gene ablation. Our analysis of both $aP2^{Cre/+}/Lpin1^{fEx2\text{-}3/fEx2\text{-}3}$ (adipocyte-selective *Lpin1* knockout model) and $aP2^{Cre\text{-}ERT2/+}/Lp^{fEx2\text{-}3/fEx2\text{-}3}$ (inducible [loxP-CreER^{T2}] adipocyte-selective *Lpin1* knockout model mice) established that a cell autonomous role of lipin 1 is crucial for adipocyte maintenance and survival. We further demonstrated that intracellular PA accumulation inhibits adipocyte differentiation and contributes to the adipocyte defects observed in $aP2^{Cre/+}/Lpin1^{fEx2\text{-}3/fEx2\text{-}3}$ mice. Importantly, we also reveal that *Lpin1* expression is induced by cold exposure and contributes to thermogenic activation of brown adipose tissue (BAT). Together, these data provide new insight into the role of lipin 1 in adipocyte tissue development and function.

MATERIALS AND METHODS

Chemicals. Isobutylmethylxanthine (IBMX), dexamethasone, tamoxifen, sunflower oil, insulin, pertussis toxin, lysophosphatidic acid (LPA)

Received 19 April 2012 Returned for modification 4 May 2012
Accepted 11 September 2012
Published ahead of print 1 October 2012

Address correspondence to Karim Nadra, karim.nadra@inserm.fr, or Roman Chrast, roman.chrast@unil.ch.

* Present address: Joram D. Mul, Metabolic Diseases Institute, University of Cincinnati, Cincinnati, Ohio, USA.

Supplemental material for this article may be found at http://mcb.asm.org/.

doi:10.1128/MCB.00512-12

(oleoyl-L-a-lysophosphatidic acid sodium salt), benzamidine, phenylmethylsulfonyl fluoride (PMSF), aprotinin, leupeptin, pepstatin, Triton X-100, and phosphatidic acid (PA) (1, 2-dioctanoyl-sn-glycerol 3-phosphate sodium salt) were purchased from Sigma. Scintillation counting supplies were purchased from National Diagnostics. Rosiglitazone was obtained from Alexis Biochemicals. Radiochemicals were purchased from PerkinElmer Life Sciences. IBMX, dexamethasone, and rosiglitazone were dissolved in dimethyl sulfoxide (DMSO), PA in water, and LPA in 0.1% (wt/vol) fatty-acid-free bovine serum albumin in phosphate-buffered saline (PBS) (pH 7.2).

Cell culture and lentiviral infections. The 3T3-L1 preadipocytes were grown in high-glucose Dulbecco's modified Eagle's medium (DMEM) (Sigma) containing 10% fetal bovine serum (FBS) (Life Technologies), 100 U/ml penicillin (Gibco), and 100 mg/ml streptomycin (Gibco) at 37°C in an atmosphere of 5% CO_2 with the medium changed every second day. Adipocyte differentiation was induced as follows. At 2 days postconfluence (day 0 [D0]), the medium was changed for DMEM supplemented with 10% (vol/vol) FBS, 1 μM dexamethasone, 0.5 mM IBMX, and 1 μg/ml insulin. After 48 h (day 2), the cells were refed with DMEM containing 10% (vol/vol) FBS and 1 μg/ml insulin. From day 4, the medium consisted of DMEM with 10% (vol/vol) FBS and 1 μg/ml insulin and was changed every second day.

The human cell line, derived from an adipose depot of an infant with Simpson-Golabi-Behmel syndrome (SGBS), was cultured as previously reported (59). Briefly, confluent cells (day 0) were induced to differentiate in DMEM Ham's F-12 (1:1) medium containing 0.01 mg/ml transferrin, 100 nM cortisol, 0.2 nM triiodothyronine, and 20 nM insulin. To trigger the differentiation, 25 nM dexamethasone, 500 μM IBMX, and 2 μM rosiglitazone were present from day 0 to day 4. Intracellular accumulation of lipid droplets became evident at day 10.

Mouse embryonic fibroblasts (MEFs) were generated from 13.5-day-old embryos obtained from wild-type intercrosses. After dissection of head and visceral organs, embryos were minced and trypsinized for 30 min at 37°C. Embryonic fibroblasts were then plated and maintained in DMEM with 10% (vol/vol) FBS, 100 U/ml penicillin, and 100 mg/ml streptomycin at 37°C in an atmosphere of 5% CO_2. Adipocyte differentiation was induced as follows. At 2 days postconfluence (day 0), the medium was changed for DMEM supplemented with 10% (vol/vol) FBS, 1 μM dexamethasone, 0.5 mM IBMX, 1 μg/ml insulin, and 1 μM rosiglitazone. After 48 h (day 2), the cells were refed with DMEM containing 10% (vol/vol) FBS, 1 μg/ml insulin, and 1 μM rosiglitazone. From day 4, the medium consisted of DMEM with 10% (vol/vol) FBS, 1 μg/ml insulin, and 1 μM rosiglitazone and was changed every second day. To visualize lipid accumulation, cells were stained with Oil Red O (41). Briefly, cells were washed with PBS, fixed with 4% formaldehyde solution for 15 min at 4°C, and stained with Oil Red O for 15 min at room temperature using a 60:40 (vol/vol) dilution in water of a 0.5% stock solution (in isopropanol). Cells were then washed twice with PBS and twice with water.

Lentivirus infections were carried out using the lentiviral vector pWPI (Addgene, Cambridge, MA) carrying the green fluorescent protein (GFP) reporter gene and either no other insert (empty vector) or lipin 1β as an insert (a generous gift of Thurl Harris, University of Virginia, Charlottesville, VA). All recombinant lentiviruses were produced by transient transfection of HEK-293T cells and then purified as described previously (35). To overexpress lipin 1β, 3T3-L1 or MEF cells were infected at day 0 with either the vector expressing mouse lipin 1β or empty vector. After 48 h (day 2), the 3T3-L1 cells were refed with DMEM containing 10% FBS and 1 μg/ml insulin, and MEF cells were refed with DMEM containing 1% FBS, 1 μg/ml insulin, and 1 μM rosiglitazone.

Animals. $aP2^{Cre}$ and $aP2^{CreERT2}$ transgenic mice were obtained from Salk Institute (San Diego, CA) and IGBMC (Illkirch, France), respectively. Mice of the $aP2^{+/+}/Lpin1^{fEx2\text{-}3/fEx2\text{-}3}$, $aP2^{+/+}/Lpin1^{fEx2\text{-}3/+}$, and $aP2^{Cre/+}/Lpin1^{fEx2\text{-}3/+}$ genotypes were all referred to as "$aP2^{+/+}$" controls. $aP2^{Cre/+}/Lpin1^{fEx2\text{-}3/fEx2\text{-}3}$ and $aP2^{CreERT2/+}/Lpin1^{fEx2\text{-}3/fEx2\text{-}3}$ pups were obtained at the expected Mendelian frequency. Experiments were performed in accordance with the legal requirements of the University of Lausanne and of the Canton of Vaud (Switzerland).

Generation of $aP2^{Cre/+}/Lpin1^{fEx2\text{-}3/fEx2\text{-}3}$ and $aP2^{CreERT2/+}/Lpin1^{fEx2\text{-}3/fEx2\text{-}3}$ mice. In order to generate mice with the *Lpin1* gene selectively inactivated only in adipocytes, the $Lpin1^{fEx2\text{-}3/fEx2\text{-}3}$ mice were crossed with $aP2^{Cre}$ or $aP2^{CreERT2}$ transgenic mice (19, 22). The doubly heterozygous mice ($aP2^{Cre/+}/Lp^{fEx2\text{-}3/+}$ or $aP2^{CreERT2/+}/Lp^{fEx2\text{-}3/+}$) were crossed with homozygous $Lpin1^{fEx2\text{-}3/fEx2\text{-}3}$ mice, leading to the generation of conditional knockout mice ($aP2^{Cre/+}/Lpin1^{fEx2\text{-}3/fEx2\text{-}3}$ or $aP2^{CreERT2/+}/Lpin1^{fEx2\text{-}3/fEx2\text{-}3}$). The LpCond F (F1) and LpCond R primers were used for genotyping of the generated mice, amplifying a 780-bp product from the $Lpin1^{fEx2\text{-}3}$ allele and a 740-bp product from the $Lpin1^{+}$ allele. The aP2-CreF and aP2-CreR primer set amplifying the 492-bp PCR product was used for the detection of the $aP2^{Cre}$ allele. The combination of primers F1, F2, and R1 was used to detect $Lpin1^{\Delta Ex2\text{-}3}$ with deleted exons 2 and 3 (Fig. 1A). Detailed PCR conditions are available upon request. All primer sequences are in Table S1 in the supplemental material.

BrdU incorporation assay. Four-month-old mice were injected intraperitoneally daily for 6 consecutive days with 100 μg of BrdU per gram of body weight. The epididymal and subcutaneous white adipose tissues (WAT) were dissected, fixed in 4% paraformaldehyde for 24 h, washed in PBS, and embedded in paraffin. Paraffin sections were denatured with 2 N HCl for 20 min at 37°C and neutralized in 0.1 M sodium borate (pH 8.5) for 10 min. Sections were incubated with rat anti-BrdU (at a 1:200 dilution; Abcam) in 0.3% Triton X-100 overnight at 4°C. The next day, the sections were incubated with anti-rat secondary antibody conjugated to Alexa Fluor 594 (at a 1:200 dilution; Invitrogen) and visualized with fluorescence microscopy. The nuclei were counterstained with 4′,6-diamidino-2-phenylindole (DAPI).

Tamoxifen treatment. Four-week-old $aP2^{CreERT2/+}/Lpin1^{fEx2\text{-}3/fEx2\text{-}3}$ and $aP2^{+/+}/Lpin1^{fEx2\text{-}3/fEx2\text{-}3}$ littermates were injected intraperitoneally once a day with vehicle (sunflower oil) or with 1 mg of tamoxifen (Tamox) in 100 μl of sunflower oil for 5 consecutive days.

Cold exposure. Mice were individually housed and exposed to either 24°C or 4°C. The colonic temperature was measured with the rectal Bioseb thermometer.

High-fat-diet treatment. Under normal conditions, mice were fed a standard laboratory chow (regular diet, chow; 3.225 kcal/kg [4.9% calories from fat]; Kliba Nafag, Kaiseraugst, Switzerland). The high-fat diet (HF) study was carried out for 5 weeks with a chow containing 4.057 kcal/kg (60% calories from fat; Research Diets, New Brunswick, NJ).

Glucose tolerance test (GTT) and ITT. Male mice (ages 3 to 4 months) were fasted overnight. Glucose levels were determined 30 min before glucose injection. After an intraperitoneal (i.p.) injection of 1.5 g of glucose/kg body weight, glucose levels were determined with a OneTouch Ultra glucometer (Lifescan) at 0, 15, 30, 60, 90, and 120 min using blood from the tail vain. For the insulin tolerance test (ITT), 3- to 4-month-old randomly fed male mice were used. After an i.p. injection of 0.75 U of insulin/kg body weight (Humulin R; Eli Lilly), glucose levels were determined at 0, 15, 30, 60, 90, and 120 min as described above, and areas under the curve (AUC) were calculated.

Biochemical assays. Blood was collected in nonfasted mice from their tail or retro-orbital vein. Glucose was measured from whole blood using a Glucometer Elite meter (Bayer). Serum insulin was measured by using an enzyme-linked immunosorbent assay (ELISA) kit (Millipore Corporation, Billerica, MA). Total cholesterol, high-density lipoprotein (HDL) cholesterol, low-density lipoprotein (LDL) cholesterol, triacylglycerols, free fatty acids (FFA), and lipase were measured with a Hitachi 902 fully automated clinical analyzer (Roche Diagnostics India, Mumbai, India).

Quantitative PCR. Total RNA from sciatic nerve (peri/epineurium and endoneurium) and WAT was isolated using the Qiagen RNeasy lipid tissue kit (Qiagen), following the manufacturer's instructions. Total RNA from muscle, brain, and liver was isolated in TRIzol (Invitrogen) reagent and purified using the RNeasy kit (Qiagen). RNA quality was verified by agarose gel and/or by the Qiaxcel capillary electrophoresis device

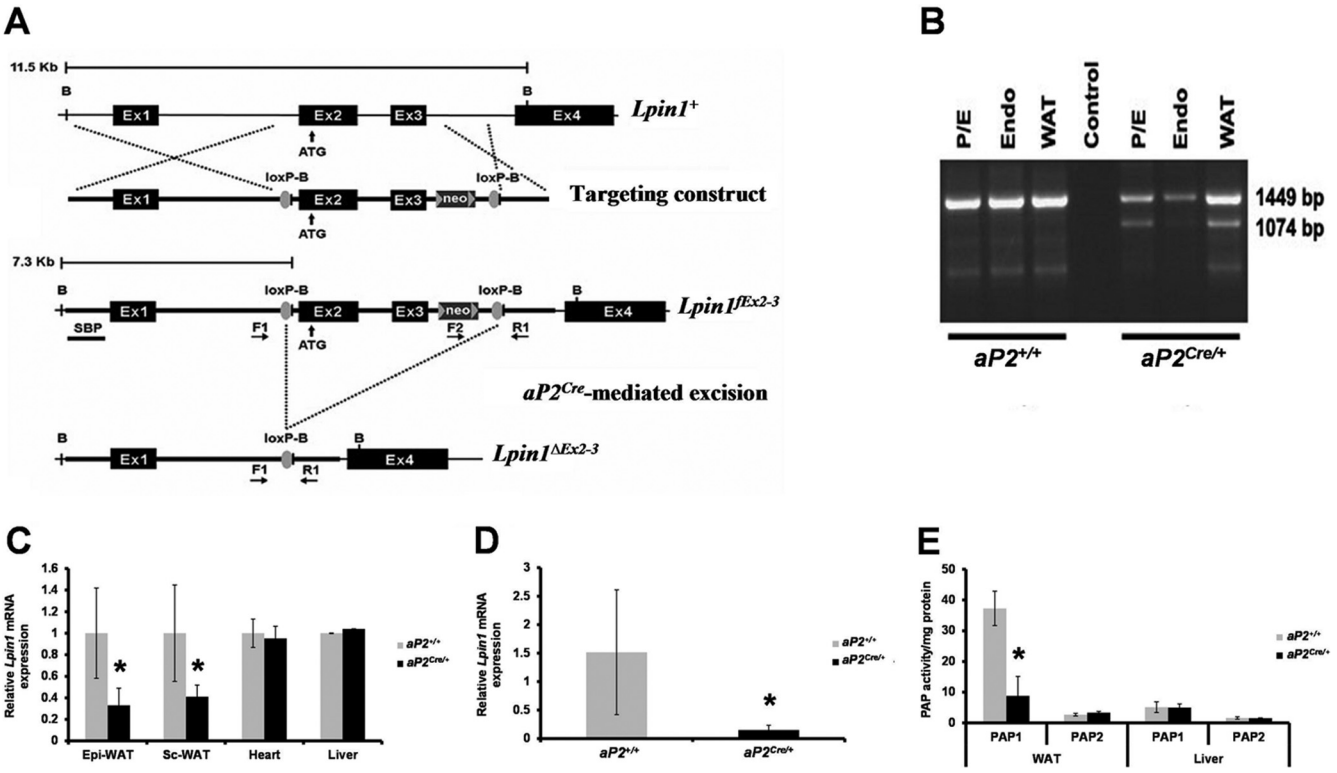

FIG 1 Adipocyte-specific deletion of *Lpin1* using an $aP2^{Cre/+}$ transgenic mouse strain. (A) Schematic overview of the wild-type *Lpin1* genomic locus ($Lpin1^{+}$), the floxed *Lpin1* allele ($Lpin1^{fEx2\text{-}3}$), and the *Lpin1*-null allele ($Lpin1^{\Delta Ex2\text{-}3}$), obtained after $aP2^{Cre}$-mediated excision. Exons are labeled as described previously (36). The F1, F2, and R1 primers were used for PCR amplification of genomic DNA. (B) *Lpin1* deletion was absent in control animals ($aP2^{+/+}$) and was observed in white adipose tissue (WAT) and the perineurial/epineurial (P/E) compartment of sciatic nerves but not in the endoneurium (Endo) from $aP2^{Cre/+}/Lpin1^{fEx2\text{-}3/fEx2\text{-}3}$ ($aP2^{Cre/+}$) mice. PCR amplification, using a combination of the primers F1, F2, and R1, was used to detect the floxed allele ($Lpin1^{fEx2\text{-}3}$; 1,449 bp) and the *Lpin1*-null allele ($Lpin1^{\Delta Ex2\text{-}3}$; 1,074 bp). (C) Quantitative PCR showed that *Lpin1* expression is decreased in epididymal (Epi) and subcutaneous (Sc) WAT whereas its expression in heart and liver was not affected in $aP2^{Cre/+}$ mice ($n = 3$; *, $P < 0.001$). (D) Quantitative PCR showed that *Lpin1* expression is almost abolished in purified $aP2^{Cre/+}$ adipocytes ($n = 4$; *, $P < 0.05$). (E) PAP1 activity was substantially decreased in WAT, but not in the liver, of $aP2^{Cre/+}$ mice compared to results for control $aP2^{+/+}$ mice. However, no significant difference in both WAT and liver PAP2 activity was observed between genotypes ($n = 8$; *, $P < 0.001$).

(Qiagen), and the concentration was determined by using an ND-1000 spectrophotometer (NanoDrop). Total RNA (250 to 500 ng) was subjected to reverse transcription using the SuperScript III First-Strand synthesis system for reverse transcription-PCR (RT-PCR) (Invitrogen), following the manufacturer's instructions. The resulting cDNA was used as a template for relative quantitative real-time PCR as described previously (36). Results were normalized using the reference gene *Ubiquitin*. See Table S1 in the supplemental material for a complete list of oligonucleotides used for RNA quantitations.

Western blotting. Tissues were lysed in ice-cold lysis buffer (20 mM $Na_2H_2PO_4$, 250 mM NaCl, Triton X-100 [1%], and SDS [0.1%]) supplemented with Complete protease inhibitor mix (Roche). Protein levels were quantified using the Bio-Rad protein assay with bovine serum albumin (BSA) as a standard. Equal amounts of protein extracts were resolved by 10% SDS-PAGE and electrotransferred onto a polyvinylidene difluoride (PVDF) membrane (Amersham Biosciences). Blots were blocked in Tris-buffered saline containing 0.1% Tween (TBS-T) supplemented with 4% milk powder and subsequently incubated overnight at 4°C in the same buffer supplemented with antibodies against Erk1/2, phosphorylated Erk1/2 (P-Erk1/2), Akt, phosphorylated Akt (P-Akt), and tubulin (Cell Signaling). After washing in TBS-T, blots were exposed to the appropriate horseradish peroxidase-conjugated secondary antibodies (Dako) in TBS-T for 1 h at room temperature. Finally, the blots were developed using ECL reagents (Pierce) and Kodak Scientific Imaging films (Kodak).

WAT fractionation. Adipocyte fractions of WAT were isolated by using a modification of a previously described protocol (26). Epididymal fat pads were excised from adult mice and placed in Hanks balanced salt solution (HBSS) (Gibco; Invitrogen) containing 1% HEPES and 3% BSA. Fat pads were finely minced, washed twice in DMEM–F-12 (Gibco; Invitrogen), and placed in DMEM–F-12 containing 1 mg/ml collagenase (type I; Worthington) at 37°C for 30 min with gentle agitation. The cell suspension was filtered through a 250-μm nylon filter (Nitex; Safar America), and the filtrate was centrifuged at 500 × *g* for 5 min at room temperature to separate the pellet containing the stromal vascular fraction (SVF) from the floating adipocytes. Total RNA was extracted from floating adipocytes using the Qiagen RNeasy lipid tissue kit (Qiagen), following the manufacturer's instructions.

PAP activity measurement. Tissue samples were disrupted using a Dounce homogenizer at 4°C in 50 mM Tris-HCl (pH 7.5) buffer containing 0.25 M sucrose, 1 mM EDTA, 10 mM β-mercaptoethanol, 1 mM benzamidine, 0.5 mM PMSF, and 5 μg/ml of aprotinin, leupeptin, and pepstatin. The lysed cells were centrifuged at 1,000 × *g* for 10 min at 4°C, and the supernatant was used as cell extract. Total PAP activity (Mg^{2+} dependent and Mg^{2+} independent) was measured at 37°C for 20 min in the reaction mixture (total volume of 100 μl) containing 50 mM Tris-HCl (pH 7.5), 1 mM $MgCl_2$, 10 mM β-mercaptoethanol, 0.2 mM [^{32}P]PA (5,000 cpm/nmol), 2 mM Triton X-100, and enzyme protein (6). The radioactive [^{32}P]PA was synthesized enzymatically from diacylglycerol and [γ-^{32}P]ATP with *Escherichia coli* diacylglycerol kinase (6). The Mg^{2+}-independent PAP activity was measured in the same reaction mixture except that 2 mM EDTA was substituted for 1 mM $MgCl_2$. Mg^{2+}-dependent PAP activity was calculated by subtracting Mg^{2+}-independent en-

zyme activity from total enzyme activity. A unit of PAP activity was defined as the amount of enzyme that catalyzed the formation of 1 nmol of product/min. Specific activity was expressed as units/mg protein. The average standard deviation of the assays was ±5%. The reactions were linear with time and protein concentration.

PA quantitation. PA was quantified as previously described (36). Tissues (the endoneurium from two nerves and ~300 mg of adipose tissue) were homogenized in 1.5 ml of PBS containing 0.5 mM Na orthovanadate (Sigma) and extracted twice with 1 volume of butanol. After evaporation, phospholipids were solubilized in 1 ml of PBS containing 1% BSA and 0.5 mM Na orthovanadate. An aliquot of the solution was incubated for 90 min at 37°C in the presence or not of bovine pancreatic PLA2 (3.8 U/ml; Sigma). At the end of the incubation, phospholipids were extracted with butanol and dried, and LPA was quantified. The amount of PA corresponds to the amount of LPA detected after treatment with PLA2 after the subtraction of the amount of LPA detected without PLA2 treatment. The assay was performed in triplicate for each sample.

WAT morphology. After measuring body weight, the left and right epididymal WAT fat pads were harvested and weighed. Subsequently, WAT samples were collected in 4% formaldehyde, rotated overnight at 4°C, rinsed twice with 100% ethanol for 2 h, left in xylene overnight at room temperature, and embedded in paraffin. The tissue was then cut in 5-μm sections and stained with hematoxylin and eosin. Average adipocyte cell diameters were measured using the NIH ImageJ software program.

RESULTS

Adipocyte-selective *Lpin1* inactivation. In order to uncover the function of lipin 1 in adipocytes, we crossed previously generated mice carrying loxP sites flanking the second and third *Lpin1* exons (*Lpin1*$^{fEx2\text{-}3/fEx2\text{-}3}$) (36) with *aP2*^{Cre} transgenic mice (Fig. 1A). *aP2*^{Cre}-mediated deletion of exons 2 and 3 is predicted to result in loss of lipin 1 function in both brown and white adipose tissue (BAT and WAT, respectively), and this strategy is expected to delete *Lpin1* throughout the formation of fat depots, thus not impairing adipocyte differentiation (19). Conditional mutant (*aP2*$^{Cre/+}$/*Lp*$^{fEx2\text{-}3/fEx2\text{-}3}$) and control (*aP2*$^{+/+}$/*Lpin1*$^{fEx2\text{-}3/fEx2\text{-}3}$ and *aP2*$^{Cre/+}$/*Lpin1*$^{fEx2\text{-}3/+}$) mice were born at the predicted Mendelian frequencies, produced normal progeny and appeared overall phenotypically normal. To examine Cre-mediated recombination efficiency, genomic DNA isolated from WAT, perineurium/epineurium, and endoneurium compartments of sciatic nerve derived from *aP2*$^{Cre/+}$/*Lp*$^{fEx2\text{-}3/fEx2\text{-}3}$ and control mice was subjected to PCR. Control mice did not show any detectable level of exon 2-exon 3 recombination. However, in the Cre-expressing mice, we detected a significant level of exon 2 and 3 deletion, specifically in adipocyte-rich peri/epineurium and WAT (Fig. 1B). As expected, aP2-driven Cre expression was high in WAT, detected in the heart, while no expression could be detected in the liver (see Fig. S1 in the supplemental material). However, the Cre expression resulted in a substantial decrease of *Lpin1* mRNA expression only in WAT and not in the heart or liver (Fig. 1C). Importantly, WAT fractionation further indicated that *Lpin1* expression in purified adipocytes derived from *aP2*$^{Cre/+}$/*Lp*$^{fEx2\text{-}3/fEx2\text{-}3}$ animals was reduced by approximately 80% compared to that for control mice (Fig. 1D). The above-mentioned results demonstrate that *Lpin1* expression was efficiently disrupted in adipocytes. Since the observed reduction of *Lpin1* expression should lead to a decrease in phosphatidic acid phosphatase (PAP1) activity (18), we measured PAP activity in WAT and liver tissue of *aP2*$^{Cre/+}$/*Lp*$^{fEx2\text{-}3/fEx2\text{-}3}$ and control mice and observed reduced PAP1 activity specifically in WAT (Fig. 1E). Interestingly, the level of PAP2 (lipid phosphate phosphatase 2) activity, which has a Mg^{2+}-independent phosphatase activity (46), was not affected in either WAT or liver derived from *aP2*$^{Cre/+}$/*Lp*$^{fEx2\text{-}3/fEx2\text{-}3}$ mice (Fig. 1E).

Functional consequences of missing lipin 1 in WAT. Although the body weight of *aP2*$^{Cre/+}$/*Lp*$^{fEx2\text{-}3/fEx2\text{-}3}$ mice was not significantly different from that of control mice on a regular diet, at 3 months of age the weight of their epididymal WAT (eWAT) fat pads was substantially lower despite normal food intake (0.19 ± 0.07 g [$n = 16$] versus 0.53 ± 0.47 g [$n = 13$]; $P = 0.007$) (Fig. 2A and C; see Fig. S2A in the supplemental material). Control mice fed a high-fat diet (HFD) showed a marked increase in body and eWAT fat pad weight (Fig. 2B and C). However, this diet-induced obesity was absent in *aP2*$^{Cre/+}$/*Lp*$^{fEx2\text{-}3/fEx2\text{-}3}$ mice (Fig. 2B and C). In line with this observation, *aP2*$^{Cre/+}$/*Lp*$^{fEx2\text{-}3/fEx2\text{-}3}$ mice showed a strong decrease in adipocyte size on both diets (Fig. 2D; see also Fig. S2B and C). In addition, numerous mature adipocytes exhibited a multilocular phenotype (fragmentation of their large lipid droplet into numerous small lipid droplets) (Fig. 2D, panel v). Although this configuration is a typical feature of brown adipocytes (9), we did not observe induction of UCP-1 mRNA expression in the WAT from *aP2*$^{Cre/+}$/*Lp*$^{fEx2\text{-}3/fEx2\text{-}3}$ mice (see Fig. S3 in the supplemental material). To test whether the multilocular cells were derived from proliferation of precursors, we treated *aP2*$^{Cre/+}$/*Lp*$^{fEx2\text{-}3/fEx2\text{-}3}$ mice with BrdU for 6 consecutive days. Although most BrdU-positive cells were endothelial and stromal cells, in *aP2*$^{Cre/+}$/*Lp*$^{fEx2\text{-}3/fEx2\text{-}3}$ mice, numerous multilocular adipocytes were labeled as well, strongly suggesting that in *aP2*$^{Cre/+}$/*Lp*$^{fEx2\text{-}3/fEx2\text{-}3}$ mice the multilocular cells derive from a mitotic proliferation of precursors (Fig. 2E and F). Albeit less frequently, this phenotype was also seen in HFD-treated animals. Because *aP2*$^{Cre/+}$/*Lp*$^{fEx2\text{-}3/fEx2\text{-}3}$ adipocytes revealed a reduction in cell size, we examined their lipid content in liver and skeletal muscle by Oil Red O staining. While no detectable changes were observed in skeletal muscle, *aP2*$^{Cre/+}$/*Lp*$^{fEx2\text{-}3/fEx2\text{-}3}$ mice developed a moderate fatty liver phenotype (see Fig. S4A in the supplemental material; also data not shown).

We next examined the effects of loss of *Lpin1* expression on metabolic parameters. As previously observed for *Lpin1*$^{fld/fld}$ mice (45), *aP2*$^{Cre/+}$/*Lp*$^{fEx2\text{-}3/fEx2\text{-}3}$ mice displayed a partial metabolic sequel of lipodystrophy. Plasma insulin levels were significantly higher in *aP2*$^{Cre/+}$/*Lp*$^{fEx2\text{-}3/fEx2\text{-}3}$ mice on regular diet or HFD, whereas glucose, cholesterol, triacylglycerols, free fatty acid (FFA), and lipase levels did not differ significantly between *aP2*$^{Cre/+}$/*Lp*$^{fEx2\text{-}3/fEx2\text{-}3}$ and control mice (Table 1). Lipodystrophy is often accompanied by insulin resistance (50); we therefore performed the intraperitoneal glucose tolerance test (ipGTT) and insulin tolerance test (ITT) with *aP2*$^{Cre/+}$/*Lp*$^{fEx2\text{-}3/fEx2\text{-}3}$ mice. While glucose levels during the ipGTT did not differ significantly between *aP2*$^{Cre/+}$/*Lp*$^{fEx2\text{-}3/fEx2\text{-}3}$ mice and control mice, the ITT revealed a significant decrease in insulin sensitivity in *aP2*$^{Cre/+}$/*Lp*$^{fEx2\text{-}3/fEx2\text{-}3}$ mice (Fig. 2G and H), indicating that the knockout animals develop insulin resistance. Together, these observations demonstrate that disruption of *Lpin1* expression in WAT results in adipocyte-selective phenotypic abnormalities during both chow and HFD feeding conditions and suggest that WAT in *aP2*$^{Cre/+}$/*Lp*$^{fEx2\text{-}3/fEx2\text{-}3}$ mice has decreased lipid storage capacity.

The absence of lipin 1 leads to defects in adipocyte maturation. To gain insight into the mechanisms underlying the *aP2*$^{Cre/+}$/*Lp*$^{fEx2\text{-}3/fEx2\text{-}3}$ phenotype, we assessed the expression of key genes involved in adipocyte biology (49). eWAT derived from

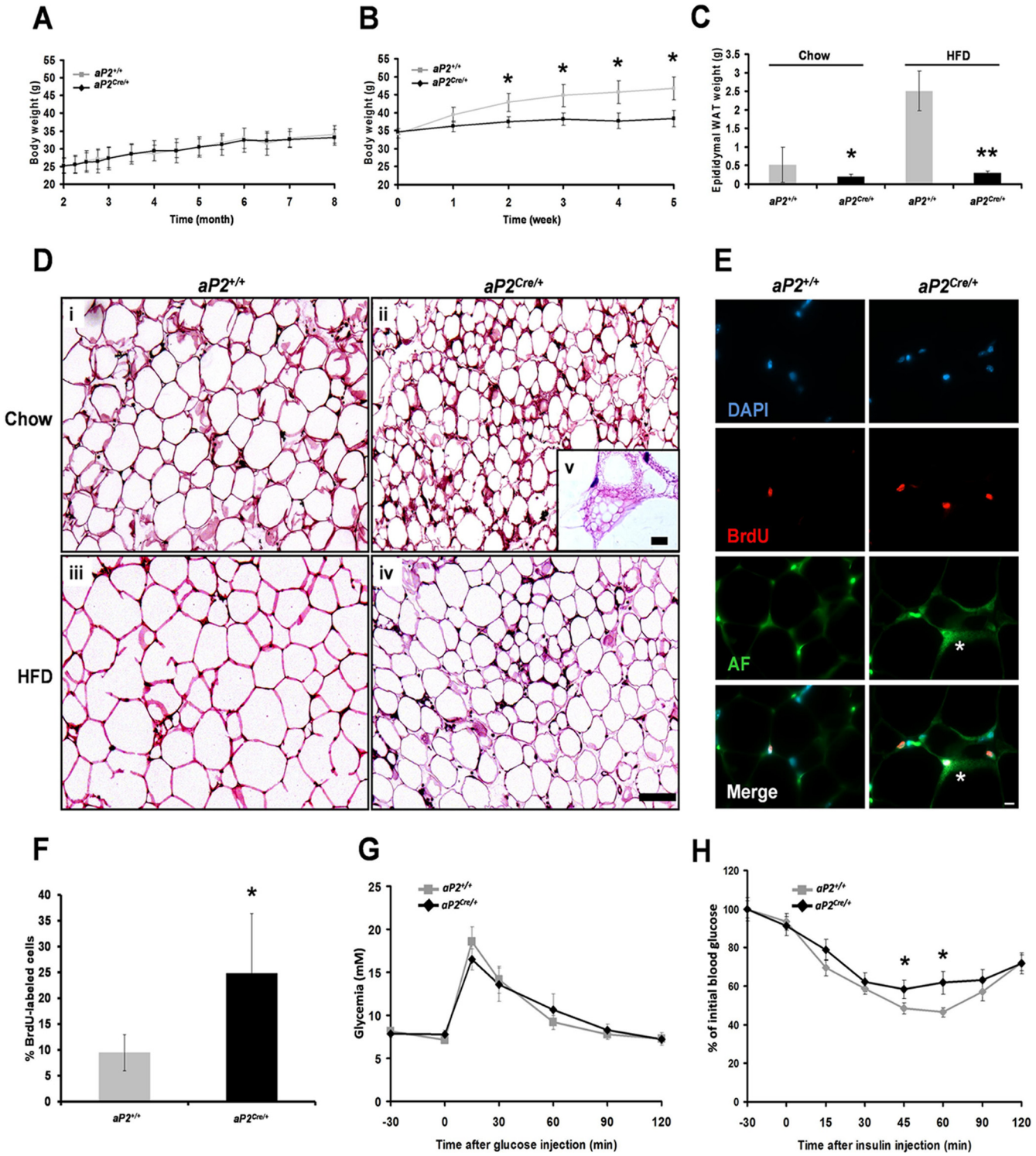

FIG 2 WAT lipodystrophy in $aP2^{Cre/+}/Lpin1^{fEx2\text{-}3/fEx2\text{-}3}$ mice. (A, B, and C) Body weight and epididymal WAT (eWAT) weight measurements in $aP2^{+/+}/Lpin1^{fEx2\text{-}3/fEx2\text{-}3}$ ($aP2^{+/+}$) and $aP2^{Cre/+}/Lpin1^{fEx2\text{-}3/fEx2\text{-}3}$ ($aP2^{Cre/+}$) mice with a regular (Chow; $n = 5$) (A and C) or high-fat (HFD; $n = 6$) (B and C) diet (*, $P < 0.05$; **, $P < 0.001$). (D) Paraffin sections of eWAT from $aP2^{+/+}$ and $aP2^{Cre/+}$ mice on chow or HFD, stained with hematoxylin and eosin. Scale bars, 100 μm (in panel iv) and 20 μm (in panel v). (E and F) BrdU immunofluorescence staining (red) (E) and determination of percentage (%) of BrdU-labeled cells (F) in WAT sections from 4-month-old $aP2^{+/+}$ and $aP2^{Cre/+}$ mice. For panel E, AF indicates the autofluorescence of adipocyte cell membranes (green). Cell nuclei are counterstained with DAPI (blue). The asterisk indicates a multilocular adipocyte labeled with BrdU. Scale bar: 10 μm. For panel F, results are expressed as mean (± SD) percentages of the number of BrdU-positive cells ($n = 4$ to 5; *, $P < 0.01$). (G and H) Blood glucose concentrations during an intraperitoneal glucose tolerance test (G) or an insulin tolerance test (H) in 4-month-old $aP2^{+/+}$ and $aP2^{Cre/+}$ mice maintained on a chow diet. In panel H, the area under the curve (AUC) represents 558 ± 87 for $aP2^{+/+}$ mice and 740 ± 178 for $aP2^{Cre/+}$ mice. Data represent means ± SD ($n = 11$ or 12; *, $P < 0.05$).

TABLE 1 Plasma glucose, insulin, lipid, and lipase levels in $aP2^{+/+}/Lp^{fE2\text{-}3/fE2\text{-}3}$ ($aP2^{+/+}$) and $aP2^{Cre/+}/Lp^{fE2\text{-}3/fE2\text{-}3}$ ($aP2^{Cre/+}$) mice on chow and high-fat diets

Metabolic parameter	Result (n) with[a]:					
	Chow diet			High-fat diet		
	$aP2^{+/+}$	$aP2^{Cre/+}$	P value	$aP2^{+/+}$	$aP2^{Cre/+}$	P value
Glucose (mmol/liter)	9.50 ± 1.65 (5)	7.30 ± 2.45 (4)	NS	9.25 ± 1.46 (6)	7.62 ± 3.37 (6)	NS
Insulin (ng/ml)	2.44 ± 1.84 (10)	7.30 ± 5.51 (5)	<0.05	7.01 ± 3.75 (6)	12.4 ± 4.24 (10)	<0.05
Total cholesterol (mmol/liter)	5.44 ± 2.24 (6)	5.52 ± 1.83 (5)	NS	7.51 ± 1.18 (5)	6.52 ± 1.62 (7)	NS
HDL cholesterol (mmol/liter)	4.26 ± 1.37 (6)	4.37 ± 1.11 (5)	NS	5.54 ± 0.64 (5)	4.85 ± 1.25 (7)	NS
LDL cholesterol (mmol/liter)	0.49 ± 0.27 (6)	0.43 ± 0.11 (5)	NS	0.61 ± 0.20 (5)	0.74 ± 0.23 (7)	NS
Triglycerides (mmol/liter)	1.37 ± 0.25 (6)	1.82 ± 0.79 (5)	NS	1.29 ± 0.27 (5)	1.51 ± 0.51 (7)	NS
Free fatty acids (mmol/liter)	0.69 ± 0.14 (6)	0.76 ± 0.30 (5)	NS	0.85 ± 0.24 (5)	0.80 ± 0.35 (7)	NS
Lipase (U/liter)	23.3 ± 7.06 (6)	27.1 ± 4.28 (5)	NS	20.1 ± 4.32 (5)	22.2 ± 3.23 (7)	NS

[a] Data represent the means ± SD (no. of mice [n] = 5 to 10) (3- to 4-month-old mice). P represents the levels of significance for differences between $aP2^{+/+}$ and $aP2^{Cre/+}$ mice by Student's t test; NS, not significantly different.

$aP2^{Cre/+}/Lp^{fEx2\text{-}3/fEx2\text{-}3}$ mice on a regular diet showed a slight but significant decrease in three markers of adipocyte maturation: fatty acid binding protein 4 (encoded by *aP2/Fabp4*), diacylglycerol acyltransferase 1 (encoded by *Dgat1*), which catalyzes the final step of the triacylglycerols synthesis (63), and *Cd36*, a facilitator of long-chain fatty acid transport (1, 10) (Fig. 3A). None of the tested markers were significantly affected by HFD feeding conditions (Fig. 3B). However, on chow we detected an increased level of expression of the macrophage markers F4/80 and CD68 in eWAT derived from $aP2^{Cre/+}/Lp^{fEx2\text{-}3/fEx2\text{-}3}$ mice (see Fig. S4B in the supplemental material).

To further study the role of lipin 1 in adipocyte maturation, mouse embryonic fibroblasts (MEFs) were derived from $aP2^{+/+}/Lp^{fEx2\text{-}3/fEx2\text{-}3}$ and $aP2^{Cre/+}/Lp^{fEx2\text{-}3/fEx2\text{-}3}$ embryos that were littermates. MEFs were induced to differentiate into adipocytes *in vitro* using a standard adipogenic induction protocol, and Oil Red O staining was performed to monitor their intracellular lipid accumulation. Importantly, the Cre expression detectable in $aP2^{Cre/+}$ cells from day 4 resulted in a substantial decrease in their *Lpin1* mRNA expression (see Fig. S5 in the supplemental material). In cells of both genotypes, oil droplets became visible on day 4 and the number of droplet-positive cells was constant until day 6 (Fig. 3C). However, at day 8, as judged by cell morphology and Oil Red O staining, the lipid droplets appeared smaller in $aP2^{Cre/+}/Lp^{fEx2\text{-}3/fEx2\text{-}3}$ MEFs, and this phenotype became more obvious at day 10. Bright-field images also revealed an accumulation of particular cell structures in $aP2^{Cre/+}/Lp^{fEx2\text{-}3/fEx2\text{-}3}$ MEFs (Fig. 3D). Coimmunostaining with adipose differentiation-related protein (ADFP) and Bodipy staining of neutral lipids revealed that these structures represent very small lipid droplets in $aP2^{Cre/+}/Lp^{fEx2\text{-}3/fEx2\text{-}3}$ MEFs (Fig. 3D, panels iv and v). In contrast, control $aP2^{+/+}/Lp^{fEx2\text{-}3/fEx2\text{-}3}$ MEFs showed enhanced differentiation with sustained lipid accumulation and characteristic morphological features of mature adipocytes, including fewer and larger lipid droplets (Fig. 3D, panel iii). These results indicate that the differentiation of $aP2^{Cre/+}/Lp^{fEx2\text{-}3/fEx2\text{-}3}$ MEFs into adipocytes induces a multilocular phenotype similar to the phenotype observed *in vivo* in WAT from $aP2^{Cre/+}/Lp^{fEx2\text{-}3/fEx2\text{-}3}$ mice. When we examined gene expression of *Pparg*, *Dgat1*, *Ucp1*, and *PGC-1α* at day 10, we observed that their expression was reduced in $aP2^{Cre/+}/Lp^{fEx2\text{-}3/fEx2\text{-}3}$ MEFs compared to that in control cells (Fig. 3E). Interestingly, we also observed reduced expression of two lipolytic genes, hormone-sensitive lipase (HSL) and adipose triglyceride lipase (ATGL) (Fig. 3E). Overall, these results suggest that the multilocular cells are preadipocytes that failed to finish their differentiation and indicate that sustained *Lpin1* expression is crucial for adipocyte maturation.

Lipin 1 plays critical role in mature white adipocytes. To specifically study the consequences of *Lpin1* inactivation in mature adipocytes, we crossed $Lpin1^{fEx2\text{-}3/fEx2\text{-}3}$ mice with $aP2^{Cre\text{-}ERT2}$ transgenic mice expressing a ligand-dependent fusion protein of Cre recombinase with a mutated ligand-binding domain of the human estrogen receptor α in white and brown adipocytes (23). Since the Cre-ER^{T2} recombinase activity is ligand dependent (22), the ablation of *Lpin1* in adipocytes of adult mice occurs only after treatment of $aP2^{Cre\text{-}ERT2/+}/Lp^{fEx2\text{-}3/fEx2\text{-}3}$ transgenic mice with tamoxifen (Tamox). One-month-old mutant ($aP2^{Cre\text{-}ERT2/+}/Lp^{fEx2\text{-}3/fEx2\text{-}3}$) and control ($aP2^{+/+}/Lp^{fEx2\text{-}3/fEx2\text{-}3}$, $aP2^{Cre\text{-}ERT2/+}/Lp^{+/fEx2\text{-}3}$, and $aP2^{Cre\text{-}ERT2/+}/Lp^{+/+}$) mice were injected with Tamox for 5 consecutive days (D0 to D4) (Fig. 4A) and characterized at days D7, D22, and D60 postinjection. PCR analysis revealed significant levels of exon 2 and 3 deletion at D7, which was less clear at D22 and D60 (Fig. 4B). The body weight of $aP2^{Cre\text{-}ERT2/+}/Lp^{fEx2\text{-}3/fEx2\text{-}3}$ mice was not different from that of control mice (see Fig. S6A in the supplemental material). However, at D7 and D22, the weight of eWAT fat pads was substantially lower in mutant animals despite normal food intake, and this phenotype disappeared at D60 (Fig. 4C; see also Fig. S6B in the supplemental material). While control $aP2^{+/+}/Lp^{fEx2\text{-}3/fEx2\text{-}3}$ eWAT was composed of characteristic large, unilocular triglyceride-filled adipocytes, histology of eWAT from $aP2^{Cre\text{-}ERT2/+}/Lp^{fEx2\text{-}3/fEx2\text{-}3}$ mice at D7 and D22 revealed a strong reduction of unilocular adipocyte size and frequent areas of multilocular cell clusters (Fig. 4D; see also Fig. S6C and D). Importantly, at D60, the multilocular cells were rarely observed in eWAT from $aP2^{Cre\text{-}ERT2/+}/Lp^{fEx2\text{-}3/fEx2\text{-}3}$ mice, indicating that a mechanism of adipose tissue recovery occurred between D22 and D60. In addition, as observed for the $aP2^{Cre/+}/Lp^{fEx2\text{-}3/fEx2\text{-}3}$ mice, at D60 the mean number of cells per field was significantly higher in $aP2^{Cre\text{-}ERT2/+}/Lp^{fEx2\text{-}3/fEx2\text{-}3}$ eWAT than in the control $aP2^{+/+}/Lp^{fEx2\text{-}3/fEx2\text{-}3}$ eWAT, confirming that the reduced tissue mass reflects a reduction in cell size (see Fig. S6C). We further evaluated the adipocyte phenotype by measuring the level of expression of selected adipocyte markers in purified epididymal adipocytes

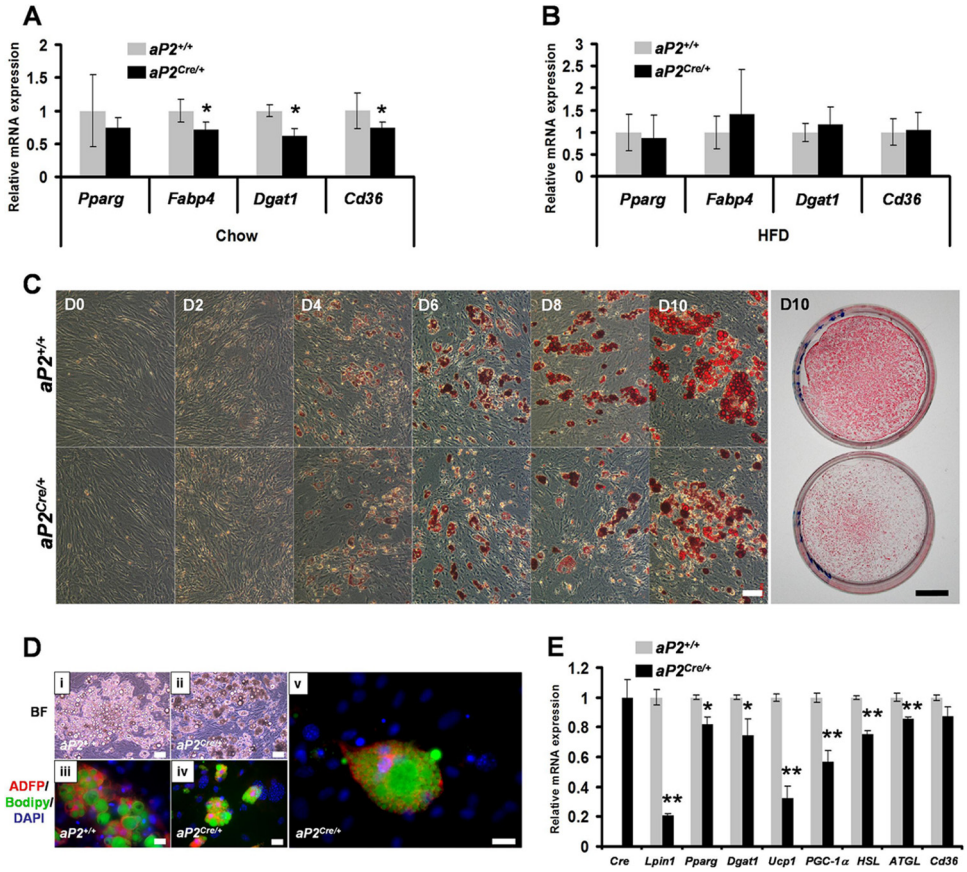

FIG 3 *In vivo* and *ex vivo* characterizations of $aP2^{Cre/+}/Lpin1^{fEx2\text{-}3/fEx2\text{-}3}$ adipocytes. (A and B) Quantitative PCR measurement of *Pparg*, *Fabp4*, *Dgat1*, and *Cd36* expression in purified eWAT adipocytes from $aP2^{+/+}$ and $aP2^{Cre/+}$ mice on chow ($n = 5$) (A) or an HFD ($n = 6$) (B) (*, $P < 0.05$). (C) Confluent $aP2^{+/+}/Lpin1^{fEx2\text{-}3/fEx2\text{-}3}$ ($aP2^{+/+}$) and $aP2^{Cre/+}/Lpin1^{fEx2\text{-}3/fEx2\text{-}3}$ ($aP2^{Cre/+}$) MEFs were exposed to differentiation medium for 2 days (D) and then cultured for 0, 2, 4, 6, 8, and 10 days in the growth medium containing insulin. Oil Red O staining of $aP2^{+/+}$ and $aP2^{Cre/+}$ MEFs at 0, 2, 6, 8, and 10 days of differentiation is shown. Scale bars, 100 μm and 1 cm. (D) Differentiation of $aP2^{Cre/+}$ MEFs into adipocytes reproduced *in vitro* the multilocular phenotype. Bright-field pictures of $aP2^{+/+}$ (i) or $aP2^{Cre/+}$ (ii) MEFs after 10 days (D10) of differentiation are presented together with adipose differentiation-related protein (ADFP) immunostaining (red) on $aP2^{+/+}$ (iii) or $aP2^{Cre/+}$ (iv and v) MEFs. Neutral lipid droplets in the MEFs were detected by green staining with Bodipy (493/503), and DAPI (blue) was used as a nuclear counterstain. Scale bars, 100 μm (in panels i to iv) and 20 μm (in panel v). (E) Quantitative PCR measurement of the *Cre*, *Lpin1*, *Pparg*, *Dgat1*, *UCP1*, *PGC-1a*, *HSL*, *ATGL*, and *Cd36* genes in differentiation-induced $aP2^{+/+}$ and $aP2^{Cre/+}$ MEFs at D10 (data are represented as means ± SD for three independent experiments; *, $P < 0.01$; **, $P < 0.001$).

from $aP2^{Cre\text{-}ERT2/+}/Lp^{fEx2\text{-}3/fEx2\text{-}3}$ and control mice at D7, D22, and D60 (Fig. 4E). Surprisingly, while *Lpin1* mRNA levels were decreased by approximately 80% at D7 and 60% at D22, no significant difference was observed at D60, reflecting the adipocyte recovery in $aP2^{Cre\text{-}ERT2/+}/Lp^{fEx2\text{-}3/fEx2\text{-}3}$ mice. We observed a similar expression pattern for *aP2/Fabp4*, *HSL*, and *ATGL* genes (Fig. 4E). The eWAT from $aP2^{Cre\text{-}ERT2/+}/Lp^{fEx2\text{-}3/fEx2\text{-}3}$ mice also exhibited reduced expression levels of two antiapoptotic factors, *Bcl2* and *Bcl2l1* (20), potentially reflecting an increase in adipocyte cell death (Fig. 4E). In addition, we found that the mRNA level of *Wisp2*, an adipocyte precursor cell marker (8), is elevated only at D7 in eWAT from $aP2^{Cre\text{-}ERT2/+}/Lp^{fEx2\text{-}3/fEx2\text{-}3}$ mice. Interestingly, we also observed a reduced level of mRNA expression of two macrophage markers, *F4/80* and *CD68*, in eWAT from $aP2^{Cre\text{-}ERT2/+}/Lp^{fEx2\text{-}3/fEx2\text{-}3}$ mice at D60 compared to that at D7 and D22 (Fig. 4F). Collectively, these results indicate that *Lpin1* inactivation in mature adipocytes in $aP2^{Cre\text{-}ERT2/+}/Lp^{fEx2\text{-}3/fEx2\text{-}3}$ mice led to a temporally restricted lipodystrophy associated with a multilocular adipocyte phenotype, expansion of adipocyte precursor pools, and inflammation. Thus, our histological and gene expression data suggest that *Lpin1*-inactivated mature adipocytes were progressively replaced by new *Lpin1*-positive adipocytes.

Inactivation of *Lpin1* in mature adipocytes protects $aP2^{Cre\text{-}ERT2/+}/Lp^{fEx2\text{-}3/fEx2\text{-}3}$ mice against high-fat-diet-induced obesity. To evaluate the functional consequences of *Lpin1* inactivation in mature WAT, $aP2^{Cre\text{-}ERT2/+}/Lp^{fEx2\text{-}3/fEx2\text{-}3}$ mice were provided with an HFD between D60 and D130 (Fig. 4A). While weight gained by $aP2^{+/+}/Lp^{fEx2\text{-}3/fEx2\text{-}3}$ mice was substantial (~36% increase from the baseline after 10 weeks of HFD; $n = 7$), it was considerably less important in $aP2^{Cre\text{-}ERT2/+}/Lp^{fEx2\text{-}3/fEx2\text{-}3}$ mice (~15%; $n = 6$) (Fig. 5A) despite having equal food intake (data not shown). The decreased weight gain of $aP2^{Cre\text{-}ERT2/+}/Lp^{fEx2\text{-}3/fEx2\text{-}3}$ mice was reflected by lower eWAT weight and less-substantial increases in eWAT adipocyte size (Fig. 5B to D). This indicates that fat storage in adipocytes is altered in $aP2^{Cre\text{-}ERT2/+}/Lp^{fEx2\text{-}3/fEx2\text{-}3}$ mice. More importantly, the increase in adipocyte cell size seen in control $aP2^{+/+}/Lp^{fEx2\text{-}3/fEx2\text{-}3}$ mice was accompa-

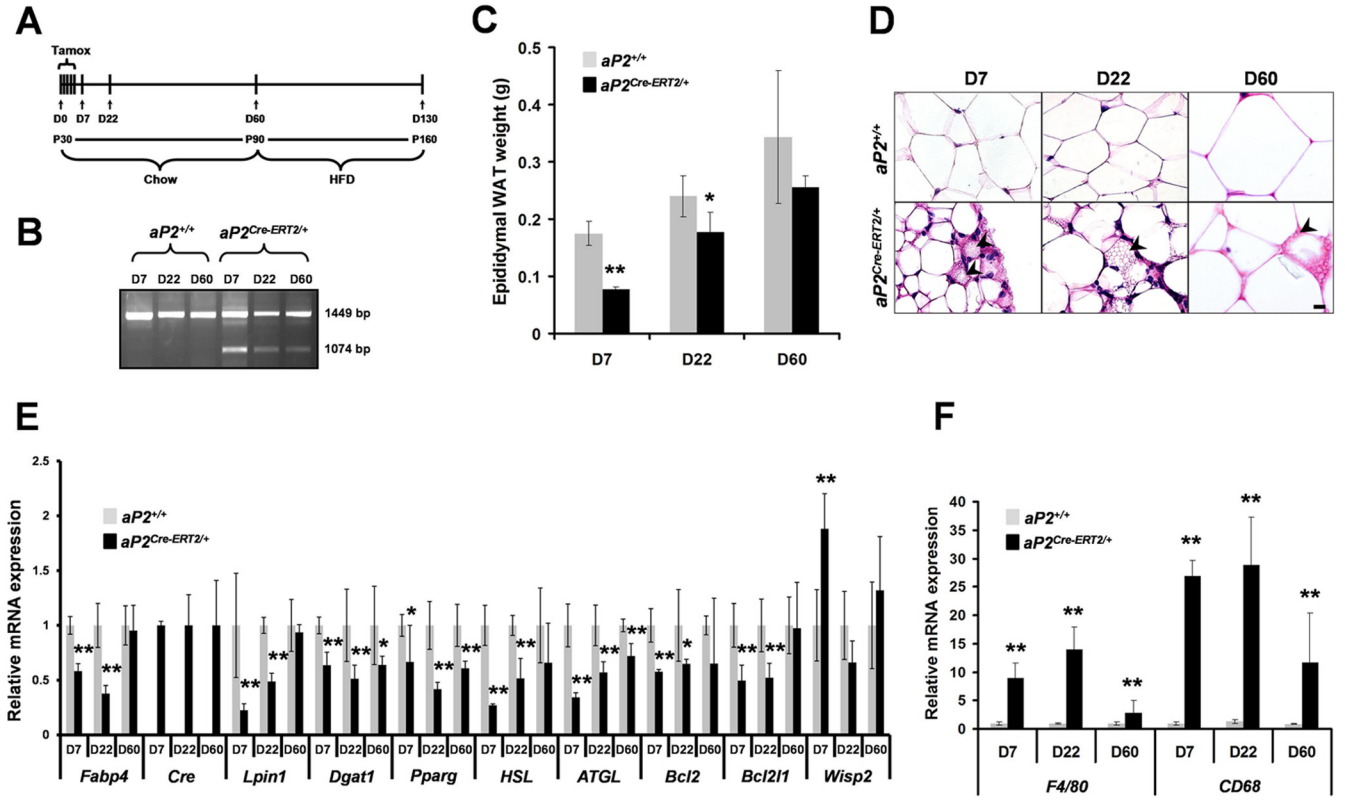

FIG 4 Consequences of *Lpin1* inactivation in mature adipocytes in $aP2^{Cre\text{-}ERT2/+}/Lpin1^{fEx2\text{-}3/fEx2\text{-}3}$ mice. (A) Timing of Tamox administration and phenotypic analysis. D0 to D7, days of Tamox injection; P30 to P160, age in postnatal days; Chow, regular diet; HFD, high-fat diet. (B) *Lpin1* deletion was absent in control animals ($aP2^{+/+}$) and was detectable in WAT at D7 and to a lower extent at D22 and D60 in $aP2^{Cre\text{-}ERT2/+}/Lpin1^{fEx2\text{-}3/fEx2\text{-}3}$ ($aP2^{Cre\text{-}ERT2/+}$) mice. (C) eWAT weight measurements in $aP2^{+/+}/Lpin1^{fEx2\text{-}3/fEx2\text{-}3}$ ($aP2^{+/+}$) and $aP2^{Cre\text{-}ERT2/+}/Lpin1^{fEx2\text{-}3/fEx2\text{-}3}$ ($aP2^{Cre\text{-}ERT2/+}$) mice on a chow diet at D7, D22, and D60 ($n = 5$ per time point; *, $P < 0.05$; **, $P < 0.001$). (D) Paraffin sections of eWAT from $aP2^{+/+}$ and $aP2^{Cre\text{-}ERT2/+}$ mice on a chow diet, stained with hematoxylin and eosin. Arrowheads indicate multilocular adipocytes. Scale bar, 10 μm. (E) Quantitative PCR measurement of *Fabp4*, *Cre*, *Lpin1*, *Dgat1*, *Pparg*, *HSL*, *ATGL*, *Bcl2*, *Bcl2l1*, and *Wisp2* expression in eWAT from $aP2^{+/+}$ and $aP2^{Cre\text{-}ERT2/+}$ mice on a chow diet at D7, D22, and D60 ($n = 5$ per time point; *, $P < 0.05$; **, $P < 0.001$). (F) Quantitative PCR measurement of *F4/80* and *CD68* expression in eWAT from $aP2^{+/+}$ and $aP2^{Cre\text{-}ERT2/+}$ mice on a chow diet at D7, D22, and D60 ($n = 5$; **, $P < 0.001$). Data represent means ± SD.

nied by an increased infiltration of macrophages in WAT and increased steatosis in the liver, both considerably less detectable in $aP2^{Cre\text{-}ERT2/+}/Lp^{fEx2\text{-}3/fEx2\text{-}3}$ mice (Fig. 5C). This observation is consistent with increased levels of mRNA expression of two macrophage markers, *F4/80* and *CD68*, in eWAT of $aP2^{+/+}/Lp^{fEx2\text{-}3/fEx2\text{-}3}$ compared to that of $aP2^{Cre\text{-}ERT2/+}/Lp^{fEx2\text{-}3/fEx2\text{-}3}$ mice at D130 on the HFD (Fig. 5E). Despite increased levels of plasma insulin at D130 in $aP2^{+/+}/Lp^{fEx2\text{-}3/fEx2\text{-}3}$ mice (Fig. 5F), no statistically significant differences were found between $aP2^{+/+}/Lp^{fEx2\text{-}3/fEx2\text{-}3}$ and $aP2^{Cre\text{-}ERT2/+}/Lp^{fEx2\text{-}3/fEx2\text{-}3}$ mice when we performed an ipGTT and ITT, indicating that glucose and insulin metabolism is normal in $aP2^{Cre\text{-}ERT2/+}/Lp^{fEx2\text{-}3/fEx2\text{-}3}$ mice at D130 on the HFD (Fig. 5G and H). We also evaluated gene expression of selected adipocyte markers (*Lpin1*, *CD36*, *Dgat1*, *aP2/Fabp4*, and *Pparg*), and we observed that none of them were significantly changed in eWAT of $aP2^{Cre\text{-}ERT2/+}/Lp^{fEx2\text{-}3/fEx2\text{-}3}$ mice (see Fig. S7 in the supplemental material). Taken together, these results indicate that the apparent protection of $aP2^{Cre\text{-}ERT2/+}/Lp^{fEx2\text{-}3/fEx2\text{-}3}$ mice from HFD consequences resulted from the smaller size of the newly differentiated white adipocytes present in $aP2^{Cre\text{-}ERT2/+}/Lp^{fEx2\text{-}3/fEx2\text{-}3}$ mice rather than from changes in their function.

Phosphatidic acid accumulates in *Lpin1*-knockout adipocytes and inhibits their differentiation. We have previously demonstrated that PA accumulates in the endoneurium of $Lpin1^{fld/fld}$ and $MPZ^{Cre/+}/Lpin1^{fEx2\text{-}3/fEx2\text{-}3}$ mice and induces Schwann cell dedifferentiation through the MEK-Erk pathway (36). These data suggest that PA might also play a role in adipocyte fate determination. Therefore, we assessed the level of PA in WAT isolated from $aP2^{Cre/+}/Lp^{fEx2\text{-}3/fEx2\text{-}3}$ mice and found that the PA level was increased 3-fold compared to that for control mice (Fig. 6A). To evaluate the possible role of PA in adipocyte differentiation, we induced 3T3-L1 cells to differentiate in the presence or absence of PA and U0126, a selective inhibitor of the MEK-Erk pathway. Oil Red O staining revealed that PA prevented differentiation of 3T3-L1 cells into adipocytes (Fig. 6B). This observation was confirmed by gene expression analysis of adipocyte-specific genes, such as *Lpin1*, *Cd36*, *Fabp4*, *Fasn*, and *Pparg* (Fig. 6C). Interestingly, inhibition of adipocyte differentiation by PA was rescued by the coadministration of U0126 (Fig. 6B and C). We confirmed the antiadipogenic activity of PA in Simpson-Golabi-Behmel syndrome (SGBS) cells, a human preadipocyte cell line (59). When SGBS cells were differentiated for 7 days in the presence of 50 μM PA in an adipogenic medium, a striking reduction in triacylglycerol droplet accumulation was observed (Fig. 6D). This effect was accompanied by a strong reduction in *Fabp4* expression (Fig. 6E). Although an increase in exogenous PA clearly

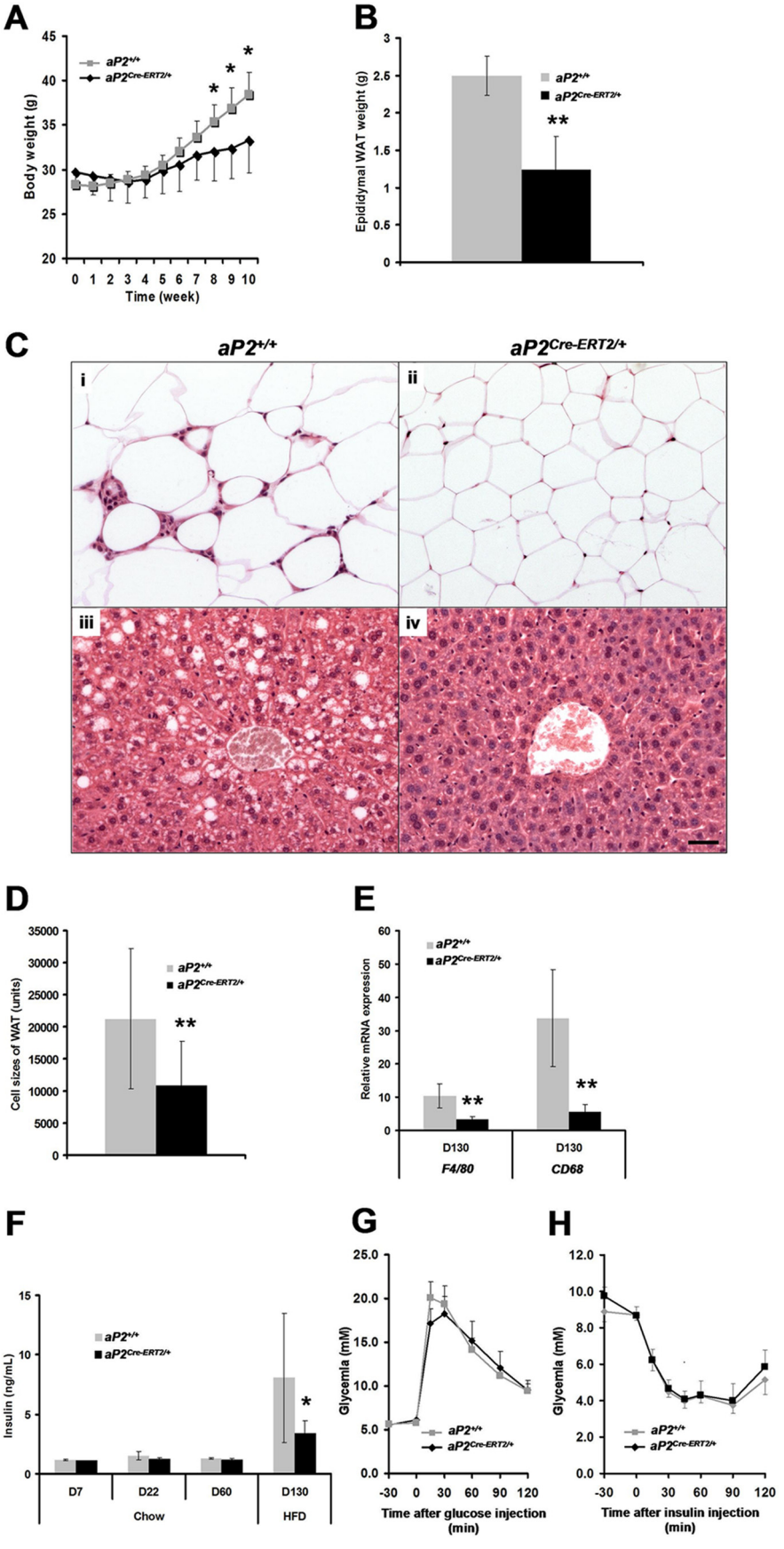
A
Body weight (g)
Time (week)
aP2+/+
aP2Cre-ERT2/+
B
Epididymal WAT weight (g)
C
aP2+/+
aP2Cre-ERT2/+
i
ii
iii
iv
D
Cell sizes of WAT (units)
E
Relative mRNA expression
D130
F4/80
CD68
F
Insulin (ng/mL)
D7
D22
D60
D130
Chow
HFD
G
Glycemia (mM)
Time after glucose injection (min)
H
Glycemia (mM)
Time after insulin injection (min)

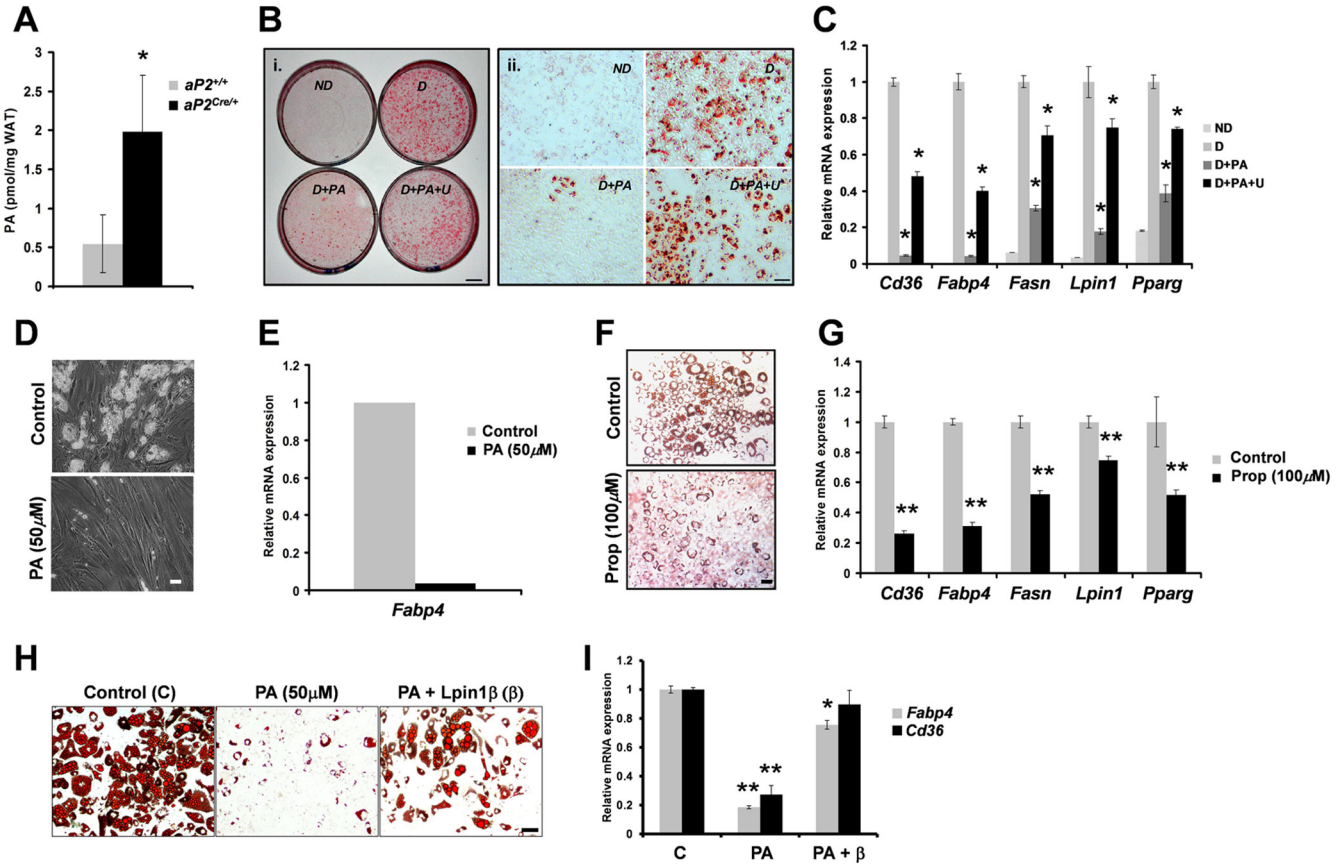

FIG 6 Phosphatidic acid prevents adipocyte differentiation. (A) PA levels in eWAT of $aP2^{Cre/+}/Lpin1^{fEx2\text{-}3/fEx2\text{-}3}$ ($aP2^{Cre/+}$) mice and $aP2^{+/+}/Lpin1^{fEx2\text{-}3/fEx2\text{-}3}$ ($aP2^{+/+}$) control mice (age, P56; $n = 5$ or 6; *, $P < 0.01$). (B) *i.* 3T3-L1 cells were induced to differentiate (D) in the presence of either 50 μM PA (D+PA) or in the presence of PA and 20 μM MEK-Erk pathway inhibitor U0126 (D+PA+U). ND, nondifferentiated cells. Cells were stained with Oil Red O. (ii) Higher magnification images of cells shown in panel i. Scale bar, 1 cm (i) or 100 μm (ii). (C) Quantitative PCR analysis of the expression of the adipocyte markers *Cd36*, *Fabp4*, *Fasn*, *Lpin1*, and *Pparg* in 3T3-L1 cells grown under conditions described for panel B. The data represent the means ± SD of triplicate measurements (*, $P < 0.001$). (D) Representative images of human Simpson-Golabi-Behmel syndrome (SGBS) preadipocyte cells induced to differentiate in the presence (PA) or absence (Control) of 50 μM PA. Scale bar, 100 μm. (E) Expression of the adipocyte marker *Fabp4*, analyzed by quantitative PCR in SGBS cells grown under conditions described for panel D. (F) Representative images of 3T3-L1 cells grown under conditions described for panel B in the absence [Control (C)] or in the presence (Prop) or absence (Control) of 100 μM propranolol. Cells were stained with Oil Red O. Scale bar, 100 μm. (G) Expression of adipocyte markers *Cd36*, *Fabp4*, *Fasn*, *Lpin1*, and *Pparg* was analyzed by quantitative PCR in 3T3-L1 cells grown under conditions described for panel F. The data represent the means ± SD of triplicate measurements (**, $P < 0.001$). (H) Representative images of 3T3-L1 cells grown under conditions described for panel B in the absence [Control (C)] or in the presence of 50 μM PA and treated either with empty vector (50 μM PA) or lipin 1β (β) [PA + Lpin1β (β)] expression-inducing viruses. Cells were stained with Oil Red O. Scale bar, 100 μm. (I) After 8 days of differentiation, the expression of adipocyte markers *Fabp4* and *Cd36* was analyzed by quantitative PCR in 3T3-L1 cells grown under conditions described for panel H. The data represent the means ± SD of triplicate measurements (*, $P < 0.01$; **, $P < 0.001$).

prevents 3T3-L1 or SGBS differentiation, the question of whether elevated endogenous PA would have the same effect on adipocyte differentiation remained unanswered by these experiments. We therefore treated 3T3-L1 cells with propranolol, a PAP1 function inhibitor that induces an intracellular accumulation of PA (14). Similar to direct treatment with PA, incubation of 3T3-L1 cells in the presence of 100 μM propranolol led to a striking reduction in accumulation of lipid droplets and in expression of *Lpin1*, *Cd36*, *Fabp4*, *Fasn*, and *Pparg* (Fig. 6F and G). Importantly, we observed that the overexpression of lipin 1β was able to rescue the effect of PA on the differentiation of 3T3-L1 cells (Fig. 6H and I). We next evaluated whether PA also affects mature adipocyte maintenance. MEFs were induced to differentiate into adipocytes and treated with 100 μM PA between D6 and D12 (see Fig. S8A in the supple-

FIG 5 $aP2^{Cre\text{-}ERT2/+}/Lpin1^{fEx2\text{-}3/fEx2\text{-}3}$ mice are resistant to HFD-induced obesity. (A and B) Body weight and eWAT weight measurements in $aP2^{+/+}/Lpin1^{fEx2\text{-}3/fEx2\text{-}3}$ ($aP2^{+/+}$) and $aP2^{Cre\text{-}ERT2/+}/Lpin1^{fEx2\text{-}3/fEx2\text{-}3}$ ($aP2^{Cre\text{-}ERT2/+}$) mice on a high-fat diet (HFD) ($n = 6$) (*, $P < 0.05$; **, $P < 0.001$). (C) Paraffin sections of eWAT (i and ii) and liver (iii and iv) from P160 (D130) $aP2^{+/+}$ and $aP2^{Cre\text{-}ERT2/+}$ mice on a HFD, stained with hematoxylin and eosin. Scale bar, 100 μm. (D) eWAT adipocyte area determined in $aP2^{+/+}$ and $aP2^{Cre\text{-}ERT2/+}$ mice on an HFD at D130 ($n = 5$ per time point; **, $P < 0.001$). (E) Quantitative PCR measurement of *F4/80* and *CD68* expression in eWAT at D130 in HFD from $aP2^{+/+}$ and $aP2^{Cre\text{-}ERT2/+}$ mice ($n = 7$ or 8; **, $P < 0.001$). (F) Plasma insulin levels at D7, D22, D60 (chow), and D130 (HFD) in $aP2^{+/+}$ and $aP2^{Cre\text{-}ERT2/+}$ mice ($n = 5$ per time point; *, $P < 0.05$). (G and H) Blood glucose concentrations during an intraperitoneal glucose tolerance test (G) or an insulin tolerance test (H) in P160 $aP2^{+/+}$ and $aP2^{Cre\text{-}ERT2/+}$ mice maintained on an HFD. Data represent means ± SD ($n = 7$ or 8).

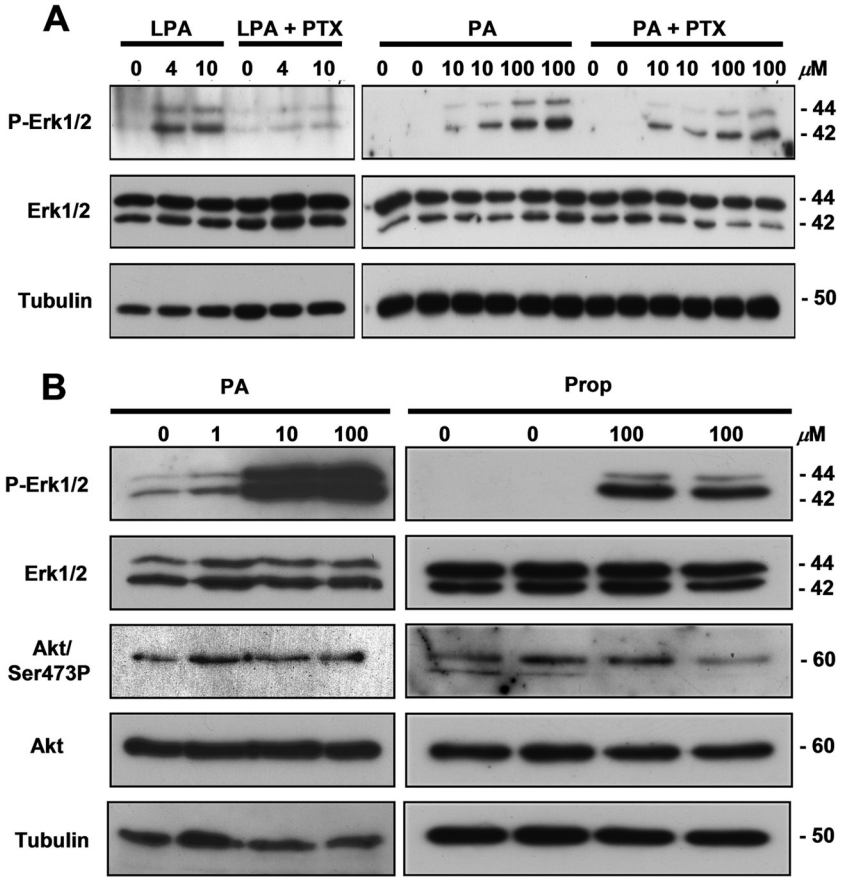

FIG 7 PA effect in adipocytes is independent of G_i protein coupled receptor. (A) 3T3-L1 cells were grown in the presence of the indicated concentration of PA or LPA or pretreated with 50 ng/ml of pertussis toxin before addition of the indicated concentration of phosphatidic acid (PA + PTX) or lysophosphatidic acid (LPA + PTX). The activation of Erk1/2 was evaluated by Western blotting using a specific antibody recognizing its phosphorylated form (P-Erk1/2). An antibody against Erk1/2 revealed its total amount in the lysate. (B) 3T3-L1 cells were treated for 1 h with increasing concentrations (0, 1, 10, and 100 μM) of PA or 100 μM of propranolol (Prop). Activation of Erk1/2 and Akt was evaluated by specific antibodies recognizing their phosphorylated forms (P-Erk1/2 and P-Akt).

mental material). Surprisingly, the number and growth of oil droplets were not disturbed, indicating that PA is not affecting mature adipocytes (see Fig. S8B). Altogether, these data suggest that the potent inhibitory effect of PA mostly plays a role in the early stage of adipocyte differentiation.

Recent reports suggested that the biological effects of exogenous PA are predominantly mediated by its conversion to lysophosphatidic acid (LPA), which subsequently activates the LPA receptor endothelial differentiation gene 2 (*Edg-2*) (62). Importantly, preadipocytes express the LPA receptor, and LPA increases preadipocyte proliferation (51). To evaluate whether the inhibitory effect of PA on 3T3-L1 cells was also mediated via LPA receptor activation, we pretreated the 3T3-L1 cells with pertussis toxin, an inhibitor of $G_{i/o}$ protein-coupled receptors (24). LPA-induced Erk1/2 phosphorylation was completely suppressed by treatment with pertussis toxin, whereas PA-induced Erk1/2 phosphorylation resisted this treatment in 3T3-L1 cells (Fig. 7A). These observations demonstrate that PA-induced Erk1/2 phosphorylation is not dependent on LPA receptor activation. Finally, in order to demonstrate the specificity of MEK-Erk signaling pathway activation by PA, we treated 3T3-L1 cells with either 1, 10, and 100 μM PA or 100 μM propranolol, the PAP1 function inhibitor, and observed a significant increase in the phosphorylation of Erk1/2, while Akt phosphorylation was not significantly affected (Fig. 7B). Together, these results suggest that intracellular PA accumulation inhibits adipocyte differentiation through the MEK-Erk pathway.

BAT development and function also require lipin 1 function. To determine the consequences of adipocyte-selective *Lpin1* disruption for BAT development in $aP2^{Cre/+}/Lp^{fEx2\text{-}3/fEx2\text{-}3}$ mice, we evaluated its structure in mutant and control mice. Macroscopic examination revealed a marked paucity of BAT in $aP2^{Cre/+}/Lp^{fEx2\text{-}3/fEx2\text{-}3}$ mice (Fig. 8A). While BAT weight was similar between $aP2^{+/+}/Lp^{fEx2\text{-}3/fEx2\text{-}3}$ and $aP2^{Cre/+}/Lp^{fEx2\text{-}3/fEx2\text{-}3}$ mice at postnatal day 10 (P10), it was considerably reduced in $aP2^{Cre/+}/Lp^{fEx2\text{-}3/fEx2\text{-}3}$ mice at P90 (~66% reduction; $n = 6$) (Fig. 8B). Active wild-type BAT consists of mitochondrion-rich eosinophilic cells containing multiple lipid droplets. In contrast, BAT derived from 3-month-old $aP2^{Cre/+}/Lp^{fEx2\text{-}3/fEx2\text{-}3}$ mice showed sparse eosinophilic staining, large unilocular vacuoles, and peripheral nuclei, resembling immature white adipocytes (Fig. 8C). To determine whether *Lpin1* ablation affected BAT function, $aP2^{Cre/+}/Lp^{fEx2\text{-}3/fEx2\text{-}3}$ and $aP2^{+/+}/Lp^{fEx2\text{-}3/fEx2\text{-}3}$ mice were exposed to cold temperatures. In contrast to control mice, which were able to maintain a correct body temperature, $aP2^{Cre/+}/Lp^{fEx2\text{-}3/fEx2\text{-}3}$ mice became hypothermic at 4°C (Fig. 8D). At 24°C, the expression of uncoupling protein 1 (encoded by *Ucp1*), the

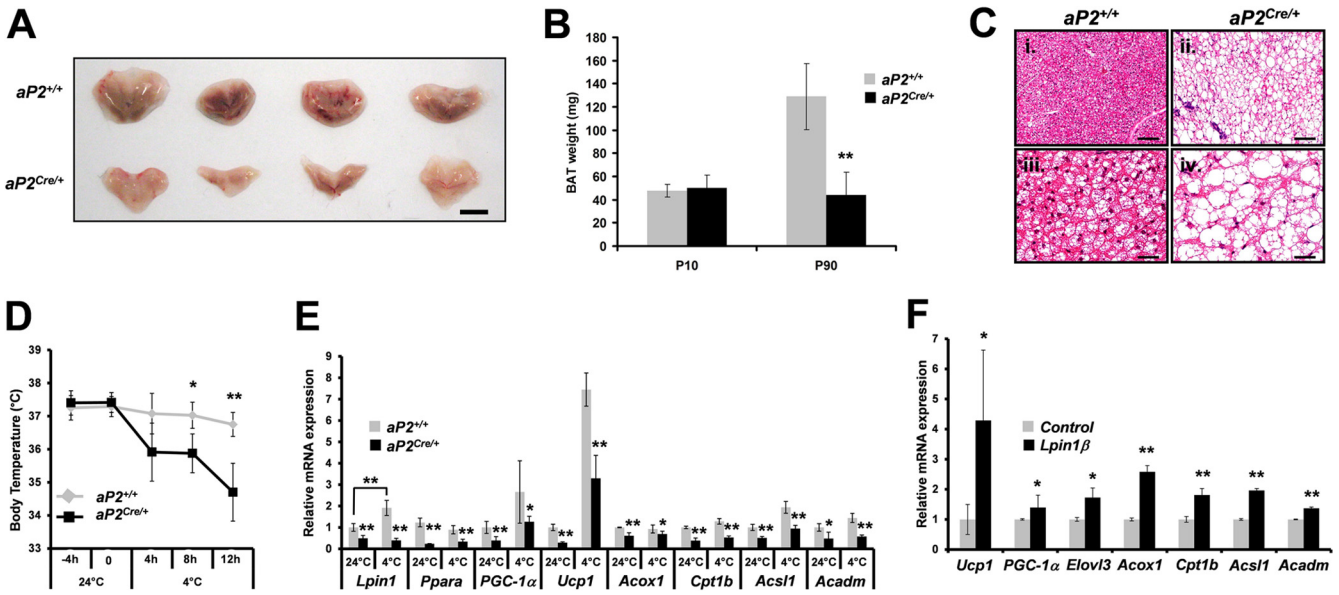

FIG 8 Lipin 1 is required for brown adipocyte development and function. (A) Representative macroscopic view of BAT isolated from 3-month-old (P90) $aP2^{+/+}/Lpin1^{fEx2\text{-}3/fEx2\text{-}3}$ ($aP2^{+/+}$) and $aP2^{Cre/+}/Lpin1^{fEx2\text{-}3/fEx2\text{-}3}$ ($aP2^{Cre/+}$) male mice. Scale bar, 5 mm. (B) BAT weight measurements in $aP2^{+/+}$ and $aP2^{Cre/+}$ P10 and P90 mice on a regular diet (Chow; $n = 5$; **, $P < 0.001$). (C) Paraffin sections prepared from BAT of $aP2^{+/+}$ and $aP2^{Cre/+}$ mice, stained with hematoxylin and eosin. Scale bar, 100 μm in (i and ii) or 25 μm (iii and iv). (D) Body temperature in $aP2^{+/+}$ and $aP2^{Cre/+}$ mice exposed to 24°C or 4°C for the indicated period of time ($n = 9$; *, $P < 0.01$; **, $P < 0.001$). (E) Quantitative PCR measurement of *Lpin1*, *Ppara*, *PGC-1α*, *Ucp1*, *Acox1*, *Cpt1b*, *Acsl1*, and *Acadm* expression in BAT from $aP2^{+/+}$ and $aP2^{Cre/+}$ mice exposed to 24°C or 4°C for 12 h ($n = 5$; *, $P < 0.01$; **, $P < 0.001$). (F) Wild-type mouse embryonic fibroblasts treated either with control (empty vector) or lipin 1β (Lpin1β) expression-inducing viruses were induced to differentiate. After 8 days of differentiation, the levels of *Ucp1*, *PGC-1α*, *Elovl3*, *Acox1*, *Cpt1b*, *Acsl1*, and *Acadm* expression were determined by quantitative PCR. The data represent the means ± SD for triplicate measurements (*, $P < 0.01$; **, $P < 0.001$; control versus Lpin1β under differentiation).

molecular marker which distinguishes BAT from WAT, as well as *PGC1-α* and *Ppara*, was strongly reduced in $aP2^{Cre/+}/Lp^{fEx2\text{-}3/fEx2\text{-}3}$ BAT compared to that for controls (Fig. 8E). PPARα is an important regulator of fatty acid oxidation (31). We therefore also examined the expression of selected PPARα target genes in the BAT of $aP2^{Cre/+}/Lp^{fEx2\text{-}3/fEx2\text{-}3}$ mice. We found that mRNA levels of several β-oxidation enzymes, including acyl coenzyme A (acyl-CoA) oxidase 1 (encoded by *Acox1*) (ACO), carnitine palmitoyltransferase 1 (encoded by *Cpt1b*) (CPT1b), long-chain acyl-CoA synthetase (encoded by *Acsl1*) (LACS), and medium-chain acyl-CoA dehydrogenase (encoded by *Acadm*) (MCAD), were markedly reduced in $aP2^{Cre/+}/Lp^{fEx2\text{-}3/fEx2\text{-}3}$ BAT compared to those for controls (Fig. 8E). These findings indicate that the capacity for β-oxidation is reduced in $aP2^{Cre/+}/Lp^{fEx2\text{-}3/fEx2\text{-}3}$ BAT.

As expected, after 12 h of exposure to 4°C, we observed a strong induction of *Ucp1* and *PGC1-α* expression in control $aP2^{+/+}/Lp^{fEx2\text{-}3/fEx2\text{-}3}$ mice. However, this upregulation was less pronounced in $aP2^{Cre/+}/Lp^{fEx2\text{-}3/fEx2\text{-}3}$ mice (Fig. 8E). Surprisingly, we observed that thermogenic activation also induces *Lpin1* gene expression in $aP2^{+/+}/Lp^{fEx2\text{-}3/fEx2\text{-}3}$ mice (Fig. 8E) concomitant with a role of lipin 1 in BAT function. To explore the effect of lipin 1 on BAT differentiation, we generated mouse embryonic fibroblast (MEF) cells overexpressing lipin 1β using a lentiviral approach. We observed that the expression of *Ucp1*, *PGC-1α*, *Elovl3* (elongation of very-long-chain fatty acid 3 [Cig30], a crucial regulator of lipid synthesis in BAT [54, 61]), *Acox1*, *Cpt1b*, *Acsl1*, and *Acadm* was higher in differentiated MEFs overexpressing lipin 1β (Fig. 8F). Together, these observations indicate that lipin 1 plays a crucial role in BAT function and differentiation.

Lipin 1 is required in mature brown adipocytes. To explore the consequences of *Lpin1* inactivation in mature brown adipocytes, we characterized intracapsular BAT (iBAT) in $aP2^{Cre\text{-}ERT2/+}/Lp^{fEx2\text{-}3/fEx2\text{-}3}$ transgenic mice treated with Tamox (Fig. 4A). As observed with WAT, Tamox treatment induced significant decreases in iBAT weight in $aP2^{Cre\text{-}ERT2/+}/Lp^{fEx2\text{-}3/fEx2\text{-}3}$ mice at D7 (~30% reduction) and D22 (~52% reduction). Importantly, while still detectable, the difference in iBAT weight between $aP2^{Cre\text{-}ERT2/+}/Lp^{fEx2\text{-}3/fEx2\text{-}3}$ and $aP2^{+/+}/Lp^{fEx2\text{-}3/fEx2\text{-}3}$ mice was less pronounced (~20% reduction) at D60 (Fig. 9A). We completed these data by assessing *Lpin1*, *Cre*, and selected adipocyte marker expression in iBAT from $aP2^{Cre\text{-}ERT2/+}/Lp^{fEx2\text{-}3/fEx2\text{-}3}$ mice and control mice at D7, D22, and D60 (Fig. 9B). As expected, *Lpin1* mRNA levels were decreased by ~50% at D7 and ~32% at D22 in iBAT from $aP2^{Cre\text{-}ERT2/+}/Lp^{fEx2\text{-}3/fEx2\text{-}3}$ mice. However, no significant difference was observed at D60, reflecting a level of brown adipocyte recovery. Importantly, at D7, reduced *Lpin1* expression was associated with decreased expression of *Ucp1*, *PGC1-α*, *Ppara*, and *Pparg*, and as with *Lpin1*, the expression of these markers was normalized at D60. In agreement with these data, at D7 and D22, the histology of iBAT from $aP2^{Cre\text{-}ERT2/+}/Lp^{fEx2\text{-}3/fEx2\text{-}3}$ mice revealed much larger lipid droplets than for control mice. However, at D60, these abnormalities disappeared (Fig. 9C). Interestingly, similar to the situation observed in WAT, when we challenged the mice with an HFD (from D60 to D130), we observed that despite regular *Lpin1* and *Ucp1* expression, $aP2^{Cre/+}/Lp^{fEx2\text{-}3/fEx2\text{-}3}$ BAT had a reduced capacity to accumulate lipids (see Fig. S9 in the supplemental material). Collectively, these data revealed that lipin 1 is required for mature brown adipocyte maintenance and function.

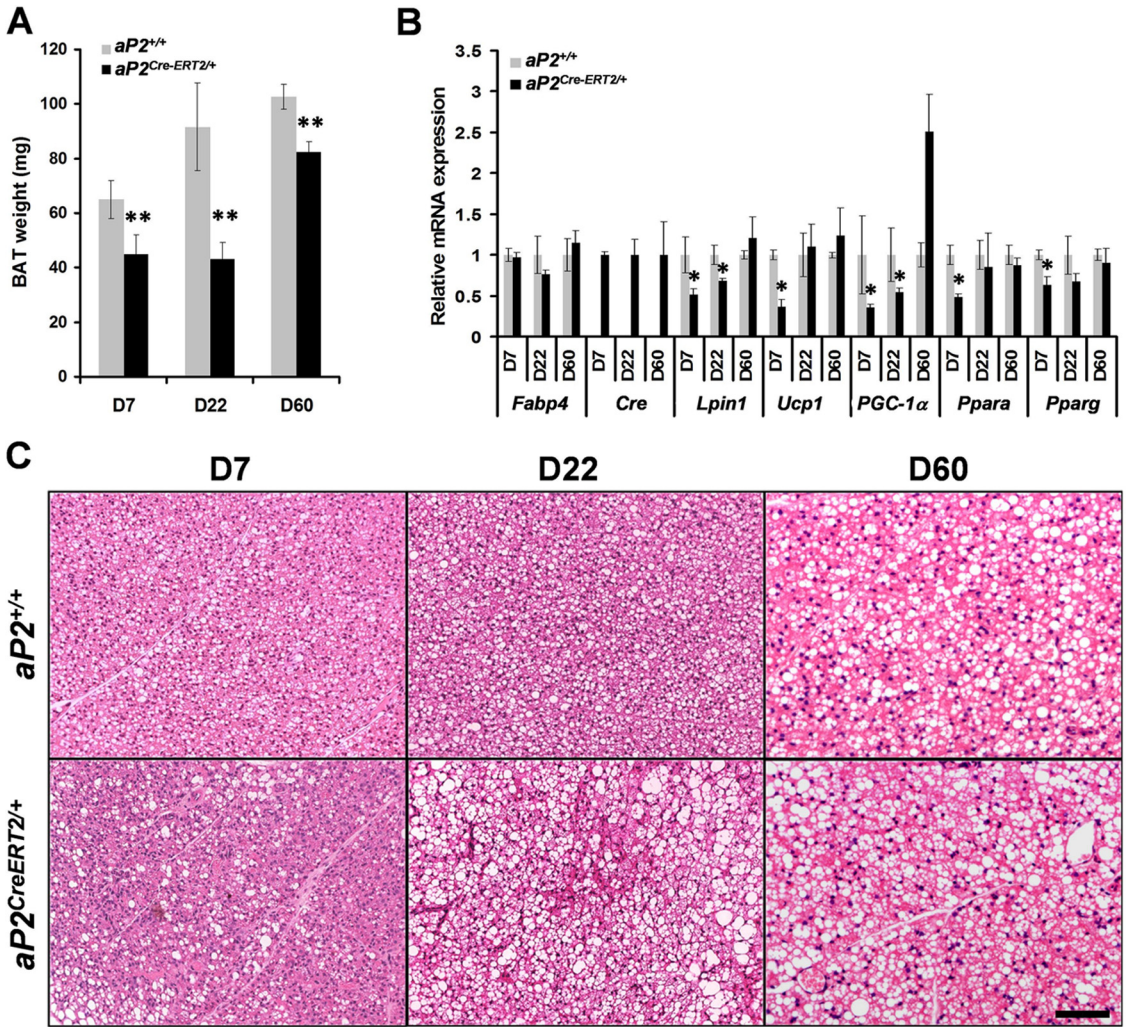

FIG 9 Lipin1 is crucial for brown adipocyte maintenance. (A) BAT weight in $aP2^{+/+}/Lpin1^{fEx2\text{-}3/fEx2\text{-}3}$ ($aP2^{+/+}$) and $aP2^{Cre\text{-}ERT2/+}/Lpin1^{fEx2\text{-}3/fEx2\text{-}3}$ ($aP2^{Cre\text{-}ERT2/+}$) mice on a chow diet at D7, D22, and D60 ($n = 5$ per time point; **, $P < 0.001$). (B) Quantitative PCR measurement of *Fabp4*, *Cre*, *Lpin1*, *Ucp1*, *PGC1*-α, *Ppara*, and *Pparg* expression in BAT from $aP2^{+/+}$ and $aP2^{Cre\text{-}ERT2/+}$ mice on a chow diet at D7, D22, and D60 ($n = 5$ per time point; *, $P < 0.001$). Data represent means ± SD. (C) Paraffin sections prepared from BAT of $aP2^{+/+}$ and $aP2^{Cre\text{-}ERT2/+}$ mice on a chow diet at D7, D22, and D60, stained with hematoxylin and eosin. Scale bar, 100 μm.

DISCUSSION

By generating and characterizing adipocyte-selective *Lpin1* knockout mice, we demonstrated a crucial cell autonomous role for lipin 1 in adipocyte function and maintenance. To study the adipocyte-selective role of lipin 1, we used two aP2-Cre lines: aP2-Cre (19) and aP2-Cre-ERT2 (22), which were bred with previously characterized floxed *Lpin1* mice (36). We showed that both aP2-Cre lines display high efficiency of Cre-mediated recombination in adipocytes. However, we also observed aP2-Cre expression in additional tissues (e.g., heart). These data confirm reports showing aP2-Cre expression in macrophages, ganglia of the peripheral nervous system, neurons of central nervous system, and certain progenitor cells during embryonic development (30, 32, 55). However, the parallel use of an inducible aP2-Cre-ERT2 line that expresses a tamoxifen-dependent Cre recombinase allow us to limit the problem of selectivity and embryonic expression of Cre, respectively. Indeed, we found that Cre-mediated inactivation of *Lpin1* leads to a multilocular adipocyte phenotype in both aP2-Cre lines and in MEFs derived from an aP2-Cre line, confirming the cell-autonomous specificity of the *Lpin1* adipocyte phenotype.

Increased *Lpin1* expression in either adipose tissue or skeletal muscle was previously demonstrated to promote obesity and to improve systemic insulin sensitivity (40). Conversely, our data showed that mice with adipocyte-selective *Lpin1* deficiency develop lipodystrophy and resistance to HFD-induced obesity. Although the resistance to obesity in aP2-Cre lines is likely related to the role of lipin 1 in triglyceride storage, the increased basal metabolic rate and total energy expenditure may also contribute to this phenotype (52), in line with the previous observation that $Lpin1^{fld/fld}$ mice exhibit higher oxygen consumption without alteration of food intake (40). These phenotypes, although less severe than with $Lpin1^{fld/fld}$ mice (45), were paralleled by insulin resistance. These *in vivo* studies thus confirmed that lower adipose *lpin1* expression is detrimental for systemic insulin sensitivity. While the association between lipodystrophy and hyperinsulin-

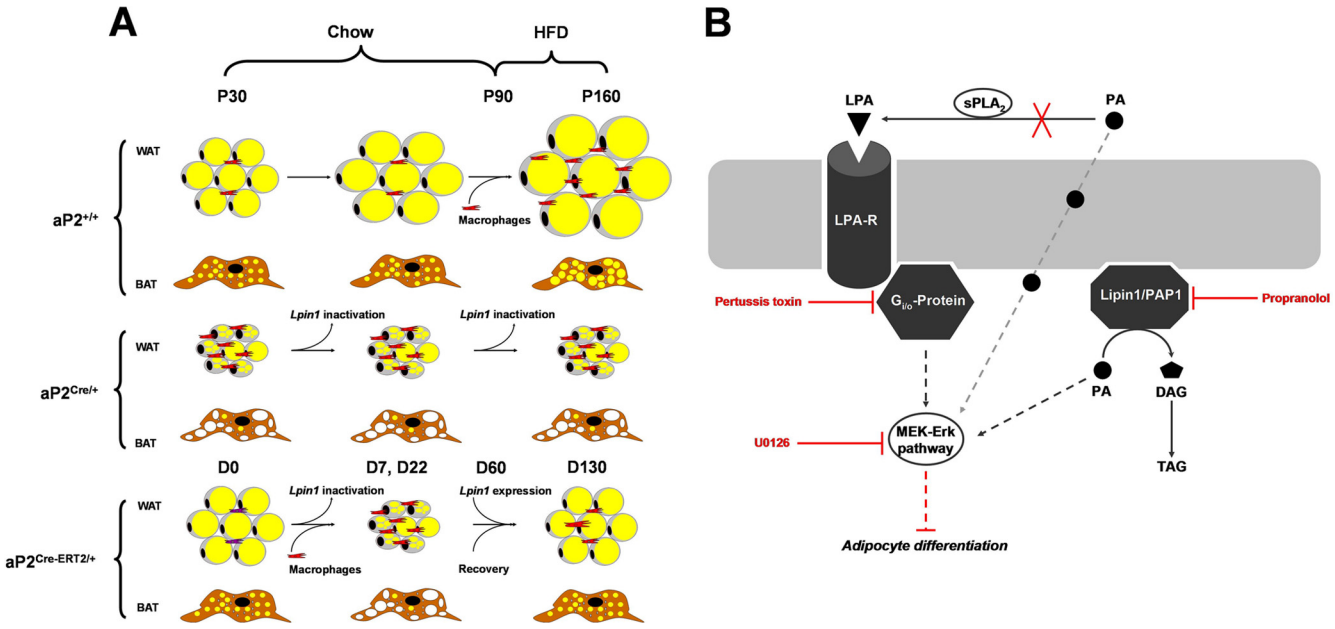

FIG 10 Role of lipin 1 in development and survival of adipocytes. (A) With a chow diet, the wild-type adipocytes accumulate lipids, leading to their increased size. This phenotype is accentuated with an HFD, leading to adipocyte inflammation, represented by the presence of macrophages (red cells). The cellular WAT morphology observed in both $aP2^{Cre/+}/Lp^{fEx2\text{-}3/fEx2\text{-}3}$ ($aP2^{Cre/+}$ at P30 to P160) and $aP2^{Cre\text{-}ERT2/+}/Lp^{fEx2\text{-}3/fEx2\text{-}3}$ ($aP2^{Cre\text{-}ERT2/+}$ at D7 to D22) mice consists of large numbers of smaller adipocytes filled with multilocular lipid droplets (yellow) accompanied by macrophage infiltration. *Lpin1* inactivation also affected the BAT structure, leading to a decreased capacity to accumulate lipids (yellow). The lipodystrophy phenotype present at D7 to D22 in WAT and BAT of $aP2^{Cre\text{-}ERT2/+}/Lp^{fEx2\text{-}3/fEx2\text{-}3}$ mice is partially recovered at D130, indicating that *Lpin1*-deficient adipocytes were replaced by newly differentiated adipocytes. Importantly, the presence of newly formed *Lpin1*-positive adipocytes in $aP2^{Cre\text{-}ERT2/+}/Lp^{fEx2\text{-}3/fEx2\text{-}3}$ mice protected them against HFD-induced adipocyte inflammation. For timing of Tamox administration ($aP2^{Cre\text{-}ERT2/+}/Lp^{fEx2\text{-}3/fEx2\text{-}3}$ mice) and phenotypic analysis, D0 (day 0) represents the first injection of Tamox which was performed at P30; P30 to P160, age in postnatal days; Chow, regular diet. (B) PA inhibits adipocyte differentiation. Accumulation of intracellular PA, either as a consequence of biochemical (propranolol) or genetic ($Lpin1^{fld/fld}$) lipin 1 inactivation, leads to activation of the MEK-Erk pathway and cell proliferation. The exogenous PA can also potentially be converted to LPA and affect adipocyte function through the $G_{i/o}$-protein LPA receptor (LPA-R) (also called EDG-2). However, biochemical inactivation (pertussis toxin) of $G_{i/o}$-protein LPA receptor does not affect the ability of extracellular PA to activate the MEK-Erk pathway, arguing against this possibility. Based on the proposed model, lipin 1/PAP-1 inactivation affects adipocytes via two mechanisms: (i) the accumulation of intracellular PA, which leads to sustained activation of the MEK-Erk pathway, affecting adipocyte differentiation, and (ii) the impairment of TAG biosynthesis.

emia was previously established (44, 50), the exact mechanism behind this phenomenon remains to be elucidated.

We further explored the consequences of *Lpin1* inactivation in matures adipocytes. While the expression of lipin 1 recovered at D60 after Tamox injection, the reduced size of the adipocytes in $aP2^{Cre\text{-}ERT2/+}/Lp^{fEx2\text{-}3/fEx2\text{-}3}$ mice indicated that *Lpin1*-deficient adipocytes were replaced by newly differentiated adipocytes (Fig. 10A). This possibility is consistent with the observation that $aP2^{Cre/+}/Lp^{fEx2\text{-}3/fEx2\text{-}3}$ WAT contains large numbers of proliferating cells compared to controls and that incorporated BrdU overlapped substantially with the multilocular adipocyte cell subpopulation. In addition, we found that the mRNA level of Wisp2, an adipocyte precursor cell marker (8, 47), was increased at D7 in $aP2^{Cre\text{-}ERT2/+}/Lp^{fEx2\text{-}3/fEx2\text{-}3}$ WAT. These findings suggest that the origin of the newly differentiated adipocytes may be either a preadipocyte or multipotent stem cell pool, which is not *Lpin1* ablated (3, 7, 48). It was previously suggested that the reduced adipocyte size plays a protective role in HFD-induced obesity. Also, adipose tissue inflammation was previously correlated with hepatic steatosis (5). In agreement with these findings, our data indicate that adipose tissue macrophage accumulation is proportional to the size of adipocytes, thus supporting the "adipose tissue expandability" hypothesis (58, 60). During HFD feeding conditions, the adipocyte tissue storage capacity or "expandability" was reached in control $aP2^{+/+}/Lp^{fEx2\text{-}3/fEx2\text{-}3}$ mice and triggered adipocyte macrophage infiltration and lipid accumulation in the liver (Fig. 10A). However, the presence of smaller adipocytes in $aP2^{Cre\text{-}ERT2/+}/Lp^{fEx2\text{-}3/fEx2\text{-}3}$ mice provided them with larger "expandability," thus contributing to observed protection against macrophage accumulation and hepatic steatosis. Together, these results suggest that pharmacological modulation of PAP1/lipin 1 activity (potentially leading to partial elimination of mature adipocytes) could be used as a strategy for prevention of obesity.

While both adipogenesis and lipogenesis are affected in $Lpin^{fld/fld}$ mice (43, 45), the integrity of adipose tissue was preserved in $aP2^{Cre/+}/Lp^{fEx2\text{-}3/fEx2\text{-}3}$ mice, and only lipid storage was affected. Part of this difference may be the consequence of the timing of $aP2^{Cre}$-driven expression (19, 23, 49). MEFs derived from $aP2^{Cre/+}/Lp^{fEx2\text{-}3/fEx2\text{-}3}$ mice are able to differentiate into adipocytes and express Cre recombinase only at the late stage of adipocyte differentiation. However, in contrast to control $aP2^{+/+}/Lp^{fEx2\text{-}3/fEx2\text{-}3}$ MEFs, the *Lpin1*-deficient MEFs lack the ability to maintain their differentiated status. The morphology and growth characteristics of these cells were altered, and similar to the *in vivo* phenotype, the $aP2^{Cre/+}/Lp^{fEx2\text{-}3/fEx2\text{-}3}$ MEFs developed a multilocular phenotype. Multilocular adipocytes appear in WAT under different conditions (17, 21, 37). For instance, rats treated with the β3-adrenoceptor agonist CL-316243 (CL) showed many multil-

ocular adipocytes with numerous small lipid droplets (typical structure of brown adipocytes), and a minority of them expressed UCP1 (21). We did not observe the expression of UCP1 (see Fig. S3 in the supplemental material), suggesting that the multilocular $aP2^{Cre/+}/Lp^{fEx2\text{-}3/fEx2\text{-}3}$ phenotype may result from dysregulation of lipolysis. However, the level of mRNA expression of HSL and ATGL, which are enzymes involved in triacylglycerol hydrolysis in adipocytes, was decreased when *Lpin1* was inactivated in adipocytes. These results suggest that the reduced accumulation of lipids/multilocular phenotype induced by *Lpin1* inactivation is mediated by an as yet unknown mechanism independent of HSL and ATGL action.

We detected large amounts of PA (the PAP1 enzyme substrate) in the white adipose tissue of $Lpin1^{fld/fld}$ (36), rat $Lpin1^{1hubr}$ (34), and adipocyte-selective *Lpin1* knockout mice (this study). This is of interest, since we previously observed that PA mediates demyelination in Schwann cell-specific *Lpin1* knockout mice (36). PA is an important lipid mediator in signal transduction of many pathways, including the mTOR and MEK-Erk pathways (2, 16). We observed, similar to the situation in Schwann cells, that PA inhibits adipocyte differentiation via the MEK-Erk pathway. This pathway was previously shown to have a dual role in adipogenesis: its activation is crucial for the early proliferative stage of adipogenesis, but the subsequent downregulation of this pathway is required for terminal adipocyte differentiation (4, 65). In contrast to what was observed in peripheral nerve tissue, PA did not affect mature adipocyte maintenance (see Fig. S8 in the supplemental material). These results thus suggest that the inhibitory effect of PA occurs mainly at an early stage of adipocyte differentiation, which may explain in part the difference between the $Lpin1^{fld/fld}$ and $aP2^{Cre/+}/Lp^{fEx2\text{-}3/fEx2\text{-}3}$ adipocyte phenotypes, since *Lpin1* inactivation (and consequently PA accumulation) occurs at a later developmental stage in $aP2^{Cre/+}/Lp^{fEx2\text{-}3/fEx2\text{-}3}$ mice. Together, these observations are in favor of the hypothesis that after adipocyte development, lipin 1 predominantly plays a role in its progressive accumulation of lipids (mediated through its role in TAG biosynthesis [Fig. 10B]) and thus in maintenance of its "unilocular" phenotype. When *Lpin1* is inactivated in $aP2^{Cre/+}/Lp^{fEx2\text{-}3/fEx2\text{-}3}$ or $aP2^{Cre\text{-}ERT2/+}/Lp^{fEx2\text{-}3/fEx2\text{-}3}$ mice, adipocytes "deflate" because their lipin 1-mediated capacity to accumulate lipids is negatively affected. Subsequently they die, to be progressively replaced by new adipocytes generated from the pool of adipocyte precursor cells.

One possible mechanism of how PA affects adipocyte development could be through its extracellular conversion to lysophosphatidic acid (LPA). LPA is known as a potent bioactive phospholipid that is able to regulate a number of cellular events, including adipogenesis (51). However, our experiments using pertussis toxin, an inhibitor of the $G_{i/o}$ protein-coupled LPA receptors, and propranolol, a lipin 1/PAP1 inhibitor, indicate that the observed adipocyte lipid storage defect in $aP2^{Cre/+}/Lp^{fEx2\text{-}3/fEx2\text{-}3}$ knockout mice is a consequence of intra-adipocyte PA accumulation (Fig. 10B).

A very striking phenotype present in both $aP2^{Cre/+}/Lp^{fEx2\text{-}3/fEx2\text{-}3}$ and $aP2^{Cre\text{-}ERT2/+}/Lp^{fEx2\text{-}3/fEx2\text{-}3}$ mice was the alteration of iBAT structure and function. The primary defects in iBAT were the loss of weight and the reduced expression of *Ucp1*, *PGC-1α*, *PPARα*, and various enzymes of the β-oxidation (*Acox1*, *Cpt1b*, *Acsl1*, and *Acadm*). We further showed that mice lacking lipin 1 are cold sensitive. These results are compatible with previous reports showing that the activation of PPARα leads to specific induction of genes involved in β-oxidation (12) and that lipin 1 activates fatty acid β-oxidation by inducing PPARα expression in the liver (15). Interestingly, we observed that thermogenic activation induces *Lpin1* gene expression. Thus, the impaired thermogenesis function in the absence of lipin 1 is likely explained by the compromised transcriptional induction of *PPARα*, *PGC-1α*, and consecutively *UCP1*. Together, these results revealed an unexpected role of lipin 1 in iBAT maintenance and function.

Lipin 1 has emerged as a crucial player in lipid metabolism, and the variation in its function was associated with both lipodystrophy and obesity (42). Herein, we demonstrated that adipocyte cell autonomous disruption of lipin 1 prevents adipocyte maturation, and we revealed the physiological relevance of the antiadipogenic activity of PA. While our data provide important insight into the relationship between defective triglyceride synthesis and lipodystrophy in the presented experimental paradigms, further experiments are needed to clarify how effectively these results replicate the etiology of human lipodystrophy. Our observation that cell autonomous inactivation of lipin 1 in mature adipocytes affects their survival and lipid accumulation strengthens the idea that adipocyte-selective lipin 1 modulation may constitute an appropriate target aiming at the prevention of metabolic disturbances in the context of obesity. Nonetheless, the adverse consequences of lipin 1 inhibition should be considered in regard to its pivotal role in other tissues, especially skeletal muscle (33, 64) and peripheral nervous system development and function (36).

ACKNOWLEDGMENTS

We thank Jean-Christophe Stehle, Janine Horlbeck, and the Mouse Metabolic Evaluation Facility platform (University of Lausanne, Lausanne, Switzerland) for technical assistance.

This work was supported by grants from the Swiss National Science Foundation to R.C. (grants PP00P3_124833/1 and 31003A_135735) and to B.D. (grant 31003A_135583/1), from the Association Française contre les Myopathies (to K.N.), and from the National Institutes of Health (grant GM-28140; to G.M.C.).

REFERENCES

1. **Abumrad NA, el-Maghrabi MR, Amri EZ, Lopez E, Grimaldi PA.** 1993. Cloning of a rat adipocyte membrane protein implicated in binding or transport of long-chain fatty acids that is induced during preadipocyte differentiation. Homology with human CD36. J. Biol. Chem. **268**:17665–17668.
2. **Andresen BT, Rizzo MA, Shome K, Romero G.** 2002. The role of phosphatidic acid in the regulation of the Ras/MEK/Erk signaling cascade. FEBS Lett. **531**:65–68.
3. **Bjorntorp P, et al.** 1978. Isolation and characterization of cells from rat adipose tissue developing into adipocytes. J. Lipid Res. **19**:316–324.
4. **Bost F, Aouadi M, Caron L, Binetruy B.** 2005. The role of MAPKs in adipocyte differentiation and obesity. Biochimie **87**:51–56.
5. **Cancello R, et al.** 2006. Increased infiltration of macrophages in omental adipose tissue is associated with marked hepatic lesions in morbid human obesity. Diabetes **55**:1554–1561.
6. **Carman GM, Lin YP.** 1991. Phosphatidate phosphatase from yeast. Methods Enzymol. **197**:548–553.
7. **Casteilla L, Dani C.** 2006. Adipose tissue-derived cells: from physiology to regenerative medicine. Diabetes Metab. **32**:393–401.
8. **Cawthorn WP, Scheller EL, MacDougald OA.** 2012. Adipose tissue stem cells meet preadipocyte commitment: going back to the future. J. Lipid Res. **53**:227–246.
9. **Cinti S.** 2011. Between brown and white: novel aspects of adipocyte differentiation. Ann. Med. **43**:104–115.

10. **Coburn CT, Hajri T, Ibrahimi A, Abumrad NA.** 2001. Role of CD36 in membrane transport and utilization of long-chain fatty acids by different tissues. J. Mol. Neurosci. **16**:117–121.
11. **Csaki LS, Reue K.** 2010. Lipins: multifunctional lipid metabolism proteins. Annu. Rev. Nutr. **30**:257–272.
12. **Desvergne B, Wahli W.** 1999. Peroxisome proliferator-activated receptors: nuclear control of metabolism. Endocr. Rev. **20**:649–688.
13. **Donkor J, Sariahmetoglu M, Dewald J, Brindley DN, Reue K.** 2007. Three mammalian lipins act as phosphatidate phosphatases with distinct tissue expression patterns. J. Biol. Chem. **282**:3450–3457.
14. **Eichberg J, Zhu X.** 1992. Diacylglycerol composition and metabolism in peripheral nerve. Adv. Exp. Med. Biol. **318**:413–425.
15. **Finck BN, et al.** 2006. Lipin 1 is an inducible amplifier of the hepatic PGC-1alpha/PPARalpha regulatory pathway. Cell Metab. **4**:199–210.
16. **Foster DA.** 2009. Phosphatidic acid signaling to mTOR: signals for the survival of human cancer cells. Biochim. Biophys. Acta **1791**:949–955.
17. **Granneman JG, Li P, Zhu Z, Lu Y.** 2005. Metabolic and cellular plasticity in white adipose tissue I: effects of beta3-adrenergic receptor activation. Am. J. Physiol. Endocrinol. Metab. **289**:E608–E616.
18. **Han GS, Wu WI, Carman GM.** 2006. The Saccharomyces cerevisiae Lipin homolog is a Mg2+-dependent phosphatidate phosphatase enzyme. J. Biol. Chem. **281**:9210–9218.
19. **He W, et al.** 2003. Adipose-specific peroxisome proliferator-activated receptor gamma knockout causes insulin resistance in fat and liver but not in muscle. Proc. Natl. Acad. Sci. U. S. A. **100**:15712–15717.
20. **Hengartner MO.** 2000. The biochemistry of apoptosis. Nature **407**:770–776.
21. **Himms-Hagen J, et al.** 2000. Multilocular fat cells in WAT of CL-316243-treated rats derive directly from white adipocytes. Am. J. Physiol. Cell Physiol. **279**:C670–C681.
22. **Imai T, Jiang M, Chambon P, Metzger D.** 2001. Impaired adipogenesis and lipolysis in the mouse upon selective ablation of the retinoid X receptor alpha mediated by a tamoxifen-inducible chimeric Cre recombinase (Cre-ERT2) in adipocytes. Proc. Natl. Acad. Sci. U. S. A. **98**:224–228.
23. **Imai T, et al.** 2004. Peroxisome proliferator-activated receptor gamma is required in mature white and brown adipocytes for their survival in the mouse. Proc. Natl. Acad. Sci. U. S. A. **101**:4543–4547.
24. **Katada T, Amano T, Ui M.** 1982. Modulation by islet-activating protein of adenylate cyclase activity in C6 glioma cells. J. Biol. Chem. **257**:3739–3746.
25. **Koh YK, et al.** 2008. Lipin1 is a key factor for the maturation and maintenance of adipocytes in the regulatory network with CCAAT/enhancer-binding protein alpha and peroxisome proliferator-activated receptor gamma 2. J. Biol. Chem. **283**:34896–34906.
26. **Koliwad SK, et al.** 2010. DGAT1-dependent triacylglycerol storage by macrophages protects mice from diet-induced insulin resistance and inflammation. J. Clin. Invest. **120**:756–767.
27. **Langner CA, et al.** 1989. The fatty liver dystrophy (fld) mutation. A new mutant mouse with a developmental abnormality in triglyceride metabolism and associated tissue-specific defects in lipoprotein lipase and hepatic lipase activities. J. Biol. Chem. **264**:7994–8003.
28. **Langner CA, Birkenmeier EH, Roth KA, Bronson RT, Gordon JI.** 1991. Characterization of the peripheral neuropathy in neonatal and adult mice that are homozygous for the fatty liver dystrophy (fld) mutation. J. Biol. Chem. **266**:11955–11964.
29. **Lindegaard B, et al.** 2007. Adipose tissue lipin expression levels distinguish HIV patients with and without lipodystrophy. Int. J. Obes. (Lond.) **31**:449–456.
30. **Makowski L, et al.** 2001. Lack of macrophage fatty-acid-binding protein aP2 protects mice deficient in apolipoprotein E against atherosclerosis. Nat. Med. **7**:699–705.
31. **Mandard S, Muller M, Kersten S.** 2004. Peroxisome proliferator-activated receptor alpha target genes. Cell. Mol. Life Sci. **61**:393–416.
32. **Martens K, Bottelbergs A, Baes M.** 2010. Ectopic recombination in the central and peripheral nervous system by aP2/FABP4-Cre mice: implications for metabolism research. FEBS Lett. **584**:1054–1058.
33. **Michot C, et al.** 2010. LPIN1 gene mutations: a major cause of severe rhabdomyolysis in early childhood. Hum. Mutat. **31**:E1564–E1573.
34. **Mul JD, et al.** 2011. A hypomorphic mutation in Lpin1 induces progressively improving neuropathy and lipodystrophy in the rat. J. Biol. Chem. **286**:26781–26793.
35. **Nadra K, et al.** 2006. Differentiation of trophoblast giant cells and their metabolic functions are dependent on peroxisome proliferator-activated receptor beta/delta. Mol. Cell. Biol. **26**:3266–3281.
36. **Nadra K, et al.** 2008. Phosphatidic acid mediates demyelination in Lpin1 mutant mice. Genes Dev. **22**:1647–1661.
37. **Narvaez CJ, Matthews D, Broun E, Chan M, Welsh J.** 2009. Lean phenotype and resistance to diet-induced obesity in vitamin D receptor knockout mice correlates with induction of uncoupling protein-1 in white adipose tissue. Endocrinology **150**:651–661.
38. **Peterfy M, Phan J, Reue K.** 2005. Alternatively spliced lipin isoforms exhibit distinct expression pattern, subcellular localization, and role in adipogenesis. J. Biol. Chem. **280**:32883–32889.
39. **Peterfy M, Phan J, Xu P, Reue K.** 2001. Lipodystrophy in the fld mouse results from mutation of a new gene encoding a nuclear protein, lipin. Nat. Genet. **27**:121–124.
40. **Phan J, Reue K.** 2005. Lipin, a lipodystrophy and obesity gene. Cell Metab. **1**:73–83.
41. **Ramirez-Zacarias JL, Castro-Munozledo F, Kuri-Harcuch W.** 1992. Quantitation of adipose conversion and triglycerides by staining intracytoplasmic lipids with Oil red O. Histochemistry **97**:493–497.
42. **Reue K.** 2009. The lipin family: mutations and metabolism. Curr. Opin. Lipidol. **20**:165–170.
43. **Reue K, Brindley DN.** 2008. Thematic review series: glycerolipids. Multiple roles for lipins/phosphatidate phosphatase enzymes in lipid metabolism. J. Lipid Res. **49**:2493–2503.
44. **Reue K, Phan J.** 2006. Metabolic consequences of lipodystrophy in mouse models. Curr. Opin. Clin. Nutr. Metab. Care **9**:436–441.
45. **Reue K, Xu P, Wang XP, Slavin BG.** 2000. Adipose tissue deficiency, glucose intolerance, and increased atherosclerosis result from mutation in the mouse fatty liver dystrophy (fld) gene. J. Lipid Res. **41**:1067–1076.
46. **Roberts RZ, Morris AJ.** 2000. Role of phosphatidic acid phosphatase 2a in uptake of extracellular lipid phosphate mediators. Biochim. Biophys. Acta **1487**:33–49.
47. **Rodeheffer MS, Birsoy K, Friedman JM.** 2008. Identification of white adipocyte progenitor cells in vivo. Cell **135**:240–249.
48. **Rodriguez AM, Elabd C, Amri EZ, Ailhaud G, Dani C.** 2005. The human adipose tissue is a source of multipotent stem cells. Biochimie **87**:125–128.
49. **Rosen ED, Walkey CJ, Puigserver P, Spiegelman BM.** 2000. Transcriptional regulation of adipogenesis. Genes Dev. **14**:1293–1307.
50. **Savage DB.** 2009. Mouse models of inherited lipodystrophy. Dis. Model. Mech. **2**:554–562.
51. **Simon MF, et al.** 2005. Lysophosphatidic acid inhibits adipocyte differentiation via lysophosphatidic acid 1 receptor-dependent down-regulation of peroxisome proliferator-activated receptor gamma2. J. Biol. Chem. **280**:14656–14662.
52. **Smith SJ, et al.** 2000. Obesity resistance and multiple mechanisms of triglyceride synthesis in mice lacking Dgat. Nat. Genet. **25**:87–90.
53. **Suviolahti E, et al.** 2006. Cross-species analyses implicate Lipin 1 involvement in human glucose metabolism. Hum. Mol. Genet. **15**:377–386.
54. **Tvrdik P, et al.** 1997. Cig30, a mouse member of a novel membrane protein gene family, is involved in the recruitment of brown adipose tissue. J. Biol. Chem. **272**:31738–31746.
55. **Urs S, Harrington A, Liaw L, Small D.** 2006. Selective expression of an aP2/fatty acid binding protein 4-Cre transgene in non-adipogenic tissues during embryonic development. Transgenic Res. **15**:647–653.
56. **van Harmelen V, Ryden M, Sjolin E, Hoffstedt J.** 2007. A role of lipin in human obesity and insulin resistance: relation to adipocyte glucose transport and GLUT4 expression. J. Lipid Res. **48**:201–206.
57. **Verheijen MH, Chrast R, Burrola P, Lemke G.** 2003. Local regulation of fat metabolism in peripheral nerves. Genes Dev. **17**:2450–2464.
58. **Virtue S, Vidal-Puig A.** 2010. Adipose tissue expandability, lipotoxicity and the Metabolic syndrome—an allostatic perspective. Biochim. Biophys. Acta **1801**:338–349.
59. **Wabitsch M, et al.** 2001. Characterization of a human preadipocyte cell strain with high capacity for adipose differentiation. Int. J. Obes. Relat. Metab. Disord. **25**:8–15.
60. **Weisberg SP, et al.** 2003. Obesity is associated with macrophage accumulation in adipose tissue. J. Clin. Invest. **112**:1796–1808.
61. **Westerberg R, et al.** 2006. ELOVL3 is an important component for early

onset of lipid recruitment in brown adipose tissue. J. Biol. Chem. **281**: 4958–4968.
62. **Winter JN, Fox TE, Kester M, Jefferson LS, Kimball SR.** 2010. Phosphatidic acid mediates activation of mTORC1 through the ERK signaling pathway. Am. J. Physiol. Cell Physiol. **299**:C335–C344.
63. **Yen CL, et al.** 2008. Thematic review series: glycerolipids. DGAT enzymes and triacylglycerol biosynthesis. J. Lipid Res. **49**:2283–2301.
64. **Zeharia A, et al.** 2008. Mutations in LPIN1 cause recurrent acute myoglobinuria in childhood. Am. J. Hum. Genet. **83**:489–494.
65. **Zhang P, Takeuchi K, Csaki LS, Reue K.** 2012. Lipin-1 phosphatidic phosphatase activity modulates phosphatidate levels to promote peroxisome proliferator-activated receptor gamma (PPARgamma) gene expression during adipogenesis. J. Biol. Chem. **287**:3485–3494.